IEEE Access
Multidisciplinary ⋮ Rapid Review ⋮ Open Access Journal

Received 7 October 2022, accepted 23 October 2022, date of publication 1 November 2022, date of current version 8 November 2022.

Digital Object Identifier 10.1109/ACCESS.2022.3218799

RESEARCH ARTICLE

Approaching K-Means for Multiantenna UAV Positioning in Combination With a Max-SIC-Min-Rate Framework to Enable Aerial IoT Networks

THANH-NAM TRAN[1], THANH-LONG NGUYEN[2], AND MIROSLAV VOZNAK[3], (Senior Member, IEEE)

[1]Faculty of Information Technology, Ton Duc Thang University, Ho Chi Minh City 70000, Vietnam
[2]Faculty of Information Technology, Ho Chi Minh City University of Food Industry, Ho Chi Minh City 70000, Vietnam
[3]Faculty of Electrical Engineering and Computer Science, Technical University of Ostrava, 708000 Ostrava, Czech Republic

Corresponding author: Thanh-Long Nguyen (longnt@hufi.edu.vn)

This work was supported in part by the Ministry of Education, Youth and Sports under Grant SP2021/25; and in part by the Large Infrastructures for Research, Experimental Development and Innovations Project under Grant LM2018140.

ABSTRACT In long-range wireless communication networks, the fading channels described in channel state information are strongly related to distance and the path loss exponent and represent a major challenge in delivering the performance required to support emerging applications. Conveniently, multiple antennas and cooperative relays are efficient solutions that can combat fading channels, thereby improving networking capacity and transmission reliability. This study investigated the use of multi-antenna unmanned aerial vehicle (UAV)s as aerial Internet of Things (IoT) relays and employed their direct line-of-sight benefits to assist IoT wireless networks. To improve the outage probability, system throughput, and energy efficiency (EE), we first considered a combination of transmit antenna selection at the transmitter and the selection combining technique at the receiver to determine the best channel from the pre-coding channel matrix. Using a practical model in a three-dimensional earth environment in combination with the K-means algorithm, we then investigated optimal UAV placement to obtain optimal channel state information for the non-orthogonal multiple access (NOMA)-IoT device cluster globally, thereby ensuring the quality of service for the IoT devices. We introduced a max-successive interference cancellation-min-rate framework for non-ordered NOMA devices, thus deriving theoretical expressions in novel closed forms for two independent scenarios: (*i*) Rayleigh and (*ii*) Nakagami-*m* fading channels. By optimizing the UAV placement, the investigated results applied to the UAV scheme delivered better performance in a NOMA-IoT network than in a terrestrial relay (TR) scheme. Finally, the study examines a variety of models and presents algorithms for Monte Carlo simulations to verify the theoretical results.

INDEX TERMS IoT wireless networks, multi-input-multi-output (MIMO), non-orthogonal multiple access (NOMA), transmit antenna selection and selection combining (TAS/SC), max-SIC-min-rate framework, UAV placement optimization, K-means algorithm.

I. INTRODUCTION

IoT networks have been employed in various smart applications such as smart homes, smart cities, smart grids, smart transportation, smart industry, smart health, etc. [1]. Researchers have already devised new concepts for future IoT wireless networks [2], [3]. IoT wireless communication networks can be supported not only by dedicated-short-range-communication (DSRC) technologies (e.g., RFID, infrared waves, Bluetooth, WiFi, etc.) but also next-generation wireless networks (i.e., beyond fifth-generation (5G) and sixth-generation (6G)) with higher network capacities, lower latency, and greater transmission distances than DSRC [4]. Three types of new service

The associate editor coordinating the review of this manuscript and approving it for publication was Jie Tang.

This work is licensed under a Creative Commons Attribution 4.0 License. For more information, see https://creativecommons.org/licenses/by/4.0/

have been proposed for networks beyond 5G/6G: universal mobile ultra-broadband (uMUB), ultra-high data density (uHDD), and ultra-high-speed and low-latency communications (uHSLLC) [5]. uMUB will enable space-aerial-terrestrial-sea area communications, uHDD will serve massive connections, and uHSLLC will provide ultra-high data transmission rates and low latency. Through emerging NOMA technology, IoT wireless communication networks can serve a large number of devices simultaneously by sharing the spectrum. For message decoding, receivers employ successive interference cancellation (SIC).

In addition to beyond 5G/6G, enabling wireless IoT networks faces other challenges in transmission distance and EE. Millimeter wave (mmWave) technique has been proposed as a key technology to satisfy the ever-growing demand for data rate due to its large bandwidth. However, the mmWave technique is challenged to achieve large coverage with only mmWave small cells deployed. A feasible scenario is that mmWave small cells are overlaid on traditional sub-6GHz networks, where the sub-6GHz provides large coverage while mmWave base stations provide high data rate transmission in wireless communication. As such, a promising solution is to deploy sub-6GHz base stations together with mmWave base stations to achieve high data rates in wireless communication networks while guaranteeing sufficient network coverage, where mmWave small cells are densely deployed to provide high-quality service [6]. To extend networking coverage, cooperative models are employed to combat fading channels, and multiple relays are often deployed instead of single relays to achieve better system performance [7], [8]. In this regard, relay selection strategies follow two main schemes. Opportunistic relay selection and partial relay selection can both be implemented as trade-offs between complexity and efficiency. Opportunistic relay selection provides the best system performance, but it requires a perfect channel state information for each relay link [9], [10], [11]. The partial relay selection scheme achieves acceptable system performance with less complexity than an opportunistic relay selection scheme because it requires only channel state information from the base station to the relay or the relay to devices [12], [13]. In adopting a threshold in the relay selection scheme, several switched-diversity combining techniques can be applied, for example, switch-and-stay combining [14], switch-and-examine combining [15], and switch-and-examine in combination with post-selection [16]. Switch-and-examine combined with post-selection has demonstrated superior performance to the other two schemes given its reduced implementation cost. Relay selection schemes in hybrid satellite-terrestrial cooperative networks have also been investigated, but only in a limited manner.

Employing multiple relays, however, might lead to greater complexity and higher hardware costs. The authors in [17] considered an uplink cooperative multi-input multi-output (MIMO)-NOMA system which was able to provide a high ergodic rate by equipping a large number of antennas at the base station, relay and two NOMA users. In [18], the authors exploited the advantage of maximum ratio combining to provide an optimal signal to interference plus noise ratio (SINR) at the receivers and leverage the MIMO technique. Maximum-ratio combining, however, may raise the receiver's complexity. To address this issue, we investigated transmit antenna selection and selection combining techniques at both the transmitter and receiver to minimize complexity and obtain optimal quality of service at the receiver.

In proposing solutions for IoT wireless communication in 5G/6G networks, UAVs are becoming increasingly attractive options for their line-of-sight benefits. UAVs and their application as aerial relays in 5G and 6G wireless communications networks is a low cost, viable solution to the problem of path-loss fading channels [19], [20]. As a flexible option, UAVs as aerial relays would be able to significantly reduce the transmission distance between the source (Src) and destination (Des) [21], [22], [23]. UAVs are not only able to assist terrestrial base stations in offloading data traffic, they can also improve the channel state information of edge devices by flying sufficiently close to provide line-of-sight connections and dynamic deployment ability [24]. In [25], the authors presented three major use cases of UAVs: (i) as base stations where infrastructure has failed or during situations of disaster; (ii) as aerial relay nodes which provide high-rate connectivity between distantly located Src-Des pairs or for short-term crowds; (iii) as aerial user equipment to collect temperature, humidity and wind strength data or for forest fire surveillance and search and rescue as remote sensing nodes in areas which are difficult to reach.

Despite the several advantages of UAV-assisted IoT wireless communication networks, some characteristics must be addressed to benefit wireless communication efficiency, i.e., air-to-air (A2A), air-to-ground (A2G) or ground-to-air (G2A) channel modeling is required. Direct UAV positioning delivers coverage and quality of service for IoT devices, but UAV allocation is challenging since the process involves three-dimensional Cartesian coordinates as opposed to two-dimensional models in traditional wireless communications networks. UAVs are allocated according to two horizontal and vertical positions [25]. Due to non-convexity, optimization on the UAV trajectory is another challenge. In some pioneering studies, researchers applied successive convex optimization [26], [27] and then reduced the complexity of the UAV trajectory [28]. Researchers have also examined optimal UAV positioning with realistic channel models [29] and combinations of solutions for block coordinate descent and successive convex approximation and also searched for possible UAV positioning strategies on two-dimensional planes. To the best of our knowledge, positioning and distances based on a flat earth have not yet been studied. We therefore investigated the latitudes and longitudes of devices on a flat earth and calculated precise ground-to-ground (G2G), A2A or A2G distances. We also exploited possible positions for UAV-IoT relays. A chaotic order of IoT devices arises after the UAV is positioned, therefore we propose applying max-SIC instead of the conventional SIC

technique to decode messages contained in the superimposed signals.

UAVs also have a major inconvenience in limited onboard energy due to the aircraft's size and weight constraints [26]. In [30], the authors proposed a solar-powered UAV and achieved an optimal trajectory. Extending the lifetime of UAVs is a significant challenge in enabling their widespread use in IoT wireless communication networks. In [2] and [31], the authors investigated an energy harvesting (EH) relay which enabled a multi-cell network to address the problem of limited power. In [32], the authors examined the rate-energy region for the achievable bit-rate threshold and residual energy in two-way decode-and-forward relay systems which applied simultaneous wireless information and power transfer (SWIPT) according to a power splitting protocol. The authors characterized rate-energy regions for both multiple access broadcast and time division broadcast protocols and also proposed a new EH relaying protocol which processed information and energy signals in multiple access broadcasts to enhance the achievable rate-energy region. The boundaries of the rate-energy regions were attained by optimizing the power splitting factor in each protocol. Efficient resource allocation schemes have also been designed to optimize network throughput and user coverage [25]. To prolong the UAV's online time, we applied the SWIPT technique in the present study. Two types of SWIPT protocol are candidates for this purpose: time switching and power splitting. In [33], the authors investigated networks which applied time switching [33](Fig. 1a) and power splitting [33](Fig. 3a). In [33](Fig. 1b) and [33](Fig. 3b), time switching needed three time slots to complete the signal propagation period, whereas power splitting required two time slots. In the present study, we selected the power splitting protocol to address EH on the UAV.

A. MOTIVATIONS AND CONTRIBUTIONS

In [34], the authors applied a combination of NOMA and SWIPT (time switching) because of its potential benefit to improve efficiency in the spectrum and EE. However, optimal EE is both non-linear and non-convex as a result of using a power allocation strategy and time switching factor. The authors therefore proposed a dual-layer algorithm to optimize the power allocation factor at the inner layer and the time switching factor at the outer layer. In [35], the authors also combined NOMA and SWIPT (power splitting) and attained system throughput at legitimate devices and intercept probability at illegitimate devices by optimizing the device bit-rate threshold and power splitting factor. Using UAVs for wireless communication is becoming increasingly attractive due to their flexibility in critical situations such as natural disasters [36]. Inspired by the above-mentioned studies, NOMA and SWIPT is a promising combination for attaining extremely low latency by servicing devices simultaneously and extending the network's lifetime by harvesting radio frequency EH and maintaining operation of the deployed UAV.

In [37], the authors investigated wireless power transfer using multi-relays and joint relay selection based on the average of a two-stage SIC [37, Eq. (18)]. Wu and Zhang also deployed multiple UAVs simultaneously to serve devices in the same transmission period [38]. However, each UAV might broadcast interference to a device served by the other UAV because the UAVs share the same radio frequency carrier. The authors therefore proposed a longer duration for the UAV to move nearer to its served devices and achieve better connections. The UAV would also fly at a sufficient distance from devices served by other UAVs to ensure minimal interference. Unfortunately, an ever-larger transmission block period leads to greater delays at the devices. Implementation of an independent multi-UAV solution leads to high hardware costs. Wireless communication networks may also experience outages in the case of only a single UAV and interruption. In the present study, we therefore propose a coupled UAV to assist the MIMO-NOMA user cluster. We investigated the deployment of a coupled UAV because its flexibility in implementation is a significant advantage over a TR. We also considered a switchable coupled UAV, where only one UAV is selected to receive and forward the signal in the transmission block period while the other UAV is inactive and harvests energy only. We also introduced a novel UAV relay selection protocol based on onboard battery voltage.

Previous studies focused on implementations of TR or UAV. The authors introduced joint optimizations based on UAV position, UAV-device links, and backhaul capacity allocation to maximize the data rate of devices in a UAV-assisted wireless network [29]. In [39], the study typically optimized an IoT network based on cluster head selection by using a modified rider optimization algorithm. The authors also considered complex cluster head selection as a relay approach for wireless sensor networks based on the shortest path and choice to select a cluster head [40]. Cluster head selection operating as a relay is not beneficial to the aerial IoT network. To illustrate, cluster head selection selects an IoT device as a relay to receive and forward signals. To the best of our knowledge, few studies have attempted to optimize UAV positioning. We cannot be certain then that the distances from the source to the cluster head and from the cluster head to devices are minimal, therefore we propose using the K-means algorithm to obtain a centroid for positioning the UAV.

Regarding the foregoing, we propose a switchable coupled UAV-assisted IoT wireless communication network that serves multiple devices simultaneously, achieves low latency, consumes less energy, reduces hardware costs and prolongs the UAV's online time. To achieve these aims, the study deployed emerging techniques and applied new concepts, contributing the following:

1) A model for a switchable coupled UAV-assisted IoT wireless communication network to serve multiple devices simultaneously by combining the emerging techniques of multi-user access from NOMA, multi-antenna, and SWIPT (power splitting protocol).

2) By applying the transmit antenna selection and selection combining techniques at the transmitters and receivers, respectively, improves outage probability performance is improved and hardware costs and algorithm complexity are reduced while retaining the benefits of multiple antennas. A novel transmit antenna selection/selection combining architecture that aids MIMO/massive MIMO (mMIMO)-NOMA networks is also outlined.
3) IoT devices are allocated at a longitude and latitude on the surface of a flat earth. The emerging SWIPT technique is applied to to prolong UAV online time. Notably, flying relay (FR)-UAV positioning is optimized according to the latitude and longitude over a flat earth environment. Using the K-means algorithm, the centroid is computed and iterated until an optimal centroid is found. To the best of our knowledge, previous studies have not considered the K-means algorithm to find the optimal position for a UAV. A general model and formulations for a MIMO-IoT network are presented in this study and may be adapted to other schemes such as single-input single-output (SISO) and mMIMO.
4) A UAV-assisted NOMA-IoT network model is examined and compared to other cooperative models (i.e., TR) over two stages (*i*) Rayleigh and (*ii*) Nakagami-*m* fading channels, and novel closed forms are obtained and then verified with Monte Carlo simulations.

B. ORGANIZATION AND NOTATION

The remainder of the paper is structured as follows: Section II outlines and formulates the coupled multi-antenna UAV-assisted IoT wireless communications model; Section III provides an analysis and presents our proposals for optimization; Section IV simulates and presents the numerical results; Section V concludes the discussion.

The paper applies the following notation:

$\mathbf{X}$ is the set of original NOMA device messages, i.e, $\mathbf{X} = \{x_1, \ldots, x_N\}$, where N is the number of devices.

$\bar{\mathbf{X}}$ contains non-decoded messages and initialization as given by $\bar{\mathbf{X}} = \mathbf{X}$.

$\hat{\mathbf{X}}$ includes decoded messages and initialization as given by $\hat{\mathbf{X}} = \emptyset$. Importantly, $\mathbf{X} = \bar{\mathbf{X}} \cup \hat{\mathbf{X}}$ and $\bar{\mathbf{X}} \cap \hat{\mathbf{X}} = \emptyset$.

$\mathbf{W}$ is the set of original message power allocation factors, i.e, $\mathbf{W} = \{\alpha_1, \ldots, \alpha_N\}$.

$\bar{\mathbf{W}}$ contains non-decoded-message power allocation factors and initialization as given by $\bar{\mathbf{W}} = \mathbf{W}$.

$\hat{\mathbf{W}}$ includes decoded-message power allocation factors and initialization as given by $\hat{\mathbf{W}} = \emptyset$. Importantly, $\mathbf{W} = \bar{\mathbf{W}} \cup \hat{\mathbf{W}}$ and $\bar{\mathbf{W}} \cap \hat{\mathbf{W}} = \emptyset$.

$[z]^+$ returns the maximum value among zero and z.

II. SYSTEM MODEL AND PROBLEM FORMULATION

The TR is a practical solution for reducing channel fading. However, if the terrain's topography is complex, constructing a TR or intelligent reflecting surface (IRS) is a challenge and may lead to high costs. In other examples, the network infrastructure may be deployed for a short period, for example, at a stadium, theatre, or concert hall, and be withdrawn shortly thereafter. It is therefore inefficient to construct a TR or IRS for this purpose. In the worst case, an unpredictable disaster may occur and destroy the facility, thereby causing network disruption. For example, the authors in [36] deployed UAV-assisted emergency networks to serve in search and rescue operations during disasters as a substitute for terrestrial infrastructure which was no longer functioning. In such cases, UAV deployment is promising as a low-cost solution with flexible deployment and ease of implementation. The study investigated the use of cooperative communications and UAVs to assist a MIMO-NOMA IoT wireless network. A scheme of the UAV network is shown in Figure 1. Importantly, the small cell IoT hub S in the model is above the surface of a flat earth, denoted $L_S^{high} = 30$ metres, and fully owns the channel state information through a multiple-user detection feature. N devices exist in a NOMA device cluster. The devices are sequenced from the nearest device D_1 to the farthest device D_N. All devices are allocated above a flat earth surface for simplicity. In other words, the height of device D_n for $n \in N$ above a flat earth is zero ($L_{D_n}^{high} = 0$ metre), as depicted in Figure 1a in [41]. The study assumed an IoT hub S, a UAV U_u ($u = \{1, 2\}$) and a device D_n ($n \in N$) equipped with the number of antennas A_S, A_{U_u} and A_{D_n}, respectively. A UAV is highly mobile. The UAV flew in a circular trajectory around the base station to select and serve a single user through joint user scheduling, as illustrated in Figure 3 in [41]. It is, however, an inconvenience that while one user is served, other users must rest. In the present study, we therefore used the emerging NOMA technique to serve multi-access simultaneously by sharing spectrum in the superimposed signal. However, the location relationship between the UAV and users impacts power allocation scheduling in addition to the SIC mechanism. For simplicity but without loss of generality, the position of the UAV was fixed after optimization. In practice, the UAV would fly continuously to find the optimal position.

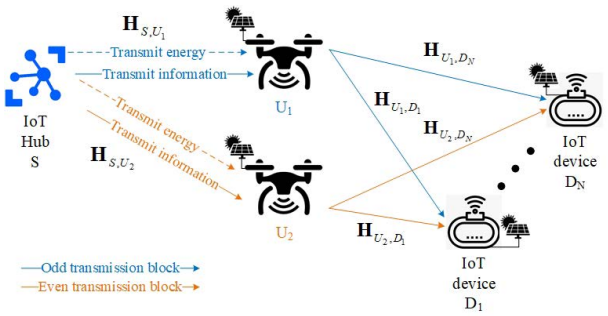

FIGURE 1. Scheme of the coupled aerial relay (UAV)-assisted MIMO-NOMA network.

A. FADING CHANNEL MODELS

In the studies [44], [45], the authors introduced a pre-coding matrix and examined a MIMO system with N_t transmit

TABLE 1. Comparisons to related works.

Studies	Antenna(s)	Relaying	Distributions	SWIPT	User(s)
[3]	Single antenna	IRS-UAV	Rayleigh	No	Single
[29]	Single antenna	Multi-UAV	Ray-tracing model	No	Multiple
[36]	Multi-antennas at UAV single antenna at devices	Multi-UAV	Nakagami-m	No	Multiple
[38]	Single	Multi-UAV	Free-space path-loss model	No	Multiple
[42]	Single antenna	UAV	Free-space path-loss model	No	Single
[43]	Multi-antennas at satellite single antenna at UAV and users	Rayleigh	Rician	No	Multiple
This study	SISO, MIMO and mMIMO	Coupled UAV	Rayleigh and Nakagami-m	Yes	Multiple

antennas and N_r (where $N_r > N_t$) receive antennas. The pre-coding channel matrix was denoted $\mathbf{H} \in \mathbb{C}^{N_r \times N_t}$ with a member $h_{i,j} \sim \mathcal{CN}(0,1)$, where $i = 1,\ldots,N_r$, $j = 1,\ldots,N_t$. $\mathbf{H}$ was known perfectly at the transmitter [44]. In [45], the authors also employed antennas N_t and N_r at the transmitter and receiver (where $N_t \geq N_r \geq 2$), and then the channel matrix under multi-user pre-coding was expressed as $\mathbf{H} = \left[\mathbf{H}_1^T \cdots \mathbf{H}_u^T \cdots \mathbf{H}_{Nu}^T\right]^T$, where $\mathbf{H}_u$ denoted the $N_r \times N_t$ MIMO channel of the u-th user. In [21], the authors considered a typical system with a narrow band condition. As shown in [21] (Fig. 1), the propagation distances of the A2G refer to the links between the aerial relay and terrestrial devices, and the propagation distances of the G2G refer to the links between terrestrial devices. These aforementioned studies applied two sequential stages t_1 and t_2 to complete a transmission block time period $t \in \left\{\mathbf{T}^{(odd)} \vee \mathbf{T}^{(even)}\right\} \subseteq \mathbf{T}$. In the first stage $t_1 \in \mathbf{T}$, the pre-coding channel matrix from IoT hub S to UAV U_u is expressed as follows:

$$\mathbf{H}_{S,U_u} = \begin{bmatrix} h_{S,U_u}^{(1,1)} & \cdots & h_{S,U_u}^{(1,A_{U_u})} \\ \vdots & \ddots & \vdots \\ h_{S,U_u}^{(A_S,1)} & \cdots & h_{S,U_u}^{(A_S,A_{U_u})} \end{bmatrix} \in \mathbb{C}^{A_S \times A_{U_u}}, \quad (1)$$

where A_S and A_{U_u} are the number of antennas on the IoT hub S and UAV U_u; the channel coefficient $h_{S,U_u}^{(a,b)} \in \mathbf{H}_{S,U_u}$ from the transmitting antenna $a \in A_S$ at the IoT hub S to the receiving antenna $b \in A_{U_u}$ at the UAV U_u is modeled according to $h_{S,U_u}^{(a,b)} = g\left(L_{S,U_u}^{A2A}\right)^{-\varepsilon}$; L_{S,U_u}^{A2A} is the A2A distance from the IoT hub S to the UAV U_u; g is the fading channel from the IoT hub S to UAV U_u (i.e., $g \sim \mathcal{CN}(0,1)$), which is distributed according to (i) Rayleigh or (ii) Nakagami-m distribution; factor ε is the path-loss exponent of the environment. The notation $\mathcal{CN}(0,1)$ presents the Gaussian distribution with zero mean and one variance. Here we have applied the free-space path-loss model mentioned in studies [3], [42], where L_{S,U_u}^{A2A} is the A2A distance from the IoT hub S to the UAV U_u and given by

$$L_{S,U_u}^{A2A} = \sqrt{\left|L_{U_u}^{high} - L_S^{high}\right|^2 + \left(L_{S,U_u}^{G2G}\right)^2}, \quad (2)$$

where G2G distance from IoT hub S to UAV U_u is obtained by substituting their latitudes and longitudes into expression (9).

In the second stage $t_2 \in \mathbf{T}$, the pre-coding channel matrix from UAV U_u to device D_n is expressed as follows:

$$\mathbf{H}_{U_u,D_n} = \begin{bmatrix} h_{U_u,D_n}^{(1,1)} & \cdots & h_{U_u,D_n}^{(1,A_{D_n})} \\ \vdots & \ddots & \vdots \\ h_{U_u,D_n}^{(A_{U_u},1)} & \cdots & h_{U_u,D_n}^{(A_{U_u},A_{D_n})} \end{bmatrix} \in \mathbb{C}^{A_{U_u} \times A_{D_n}}, \quad (3)$$

where A_{D_n} is the number of antennas on the device D_n; the channel coefficient $h_{U_u,D_n}^{(b,c)} \in \mathbf{H}_{U_u,D_n}$ is formulated according to $h_{U_u,D_n}^{(b,c)} = g\left(L_{U_u,D_n}^{A2G}\right)^{-\varepsilon}$ for $b \in A_{U_u}$ and $c \in A_{D_n}$; L_{U_u,D_n}^{A2G} is the A2G distance from the UAV U_u to the device D_n and given by

$$L_{U_u,D_n}^{A2G} = \sqrt{\left|L_{U_u}^{high} - L_{D_n}^{high}\right|^2 + \left(L_{U_u,D_n}^{G2G}\right)^2}, \quad (4)$$

where G2G the distance from the UAV U_u to device D_n is obtained by substituting their latitudes and longitudes into Eq. (9).

We examined two independent scenarios $Q = \{(i),(ii)\}$, where scenario (i) involves two-stage Rayleigh distributions and scenario (ii) involves two-stage Nakagami-m distributions.

The probability density function (PDF) and cumulative distribution function (CDF) of the Rayleigh distribution are expressed, respectively, as:

$$f_{|h_{Src,Des}|^2}(x) = \frac{1}{\sigma_{Src,Des}} \exp\left(-\frac{x}{\sigma_{Src,Des}}\right), \quad (5)$$

and

$$F_{|h_{Src,Des}|^2}(x) = 1 - \exp\left(-\frac{x}{\sigma_{Src,Des}}\right), \quad (6)$$

where $\left|h_{Src,Des}\right|^2$ are random independent variables, i.e., x in (5) and (6). In addition, $\sigma_{Src,Des}$ is the expected channel gain between Src and Des, i.e., $\sigma_{Src,Des} = E\left[\left|h_{Src,Des}\right|^2\right]$.

The PDF and CDF over Nakagami-m fading channels are expressed, respectively, as:

$$f_{|h_{Src,Des}|^2}(x) = \left(\frac{m}{\sigma_{Src,Des}}\right)^m \frac{x^{m-1}}{\Gamma(m)} \exp\left(-\frac{mx}{\sigma_{Src,Des}}\right), \quad (7)$$

and

$$F_{|h_{Src,Des}|^2}(x) = 1 - \exp\left(-\frac{mx}{\sigma_{Src,Des}}\right)$$

$$\times \sum_{j=0}^{m-1} \left(\frac{mx}{\sigma_{Src,Des}} \right)^{j} \frac{1}{j!}, \quad (8)$$

where $\Gamma(\bullet)$ in expression (7) refers to the Gamma function.

Expressions (7) and (8) are over Nakagami-m fading channels, where coefficient m is an integer value and greater than one. Expressions (7) and (8) represent expressions (5) and (6), respectively, if coefficient $m = 1$.

B. APPLYING THE K-MEANS ALGORITHM FOR UAV POSITIONING

The authors investigated social network vehicles positioned at (x, y), where x and y refer to the latitude and longitude of the vehicle, respectively, and obtained the distance between the vehicles as given by [46, Eq. (3)]. The authors also considered a UAV model with three-dimensional Cartesian coordinates (x, y, z), shown in [43] (Fig. 1), positioning the UAV over the z-axis $(0, 0, z)$ and two-devices over the x-axis $(x, 0, 0)$ or y-axis $(0, y, 0)$. They obtained the Euclidean distances from the UAV's position to these devices with [43, Eq. (1)]. Euclidean distances are complex to apply in a flat earth environment, and to the best of our knowledge have not been considered in previous studies. Without loss of generality, the study assumed one IoT hub S and a cluster of MIMO devices, including three IoT devices D_1, D_2 and D_3 positioned at the latitudes and longitudes listed in Table 2. Optimal UAV placement is also challenging due to the non-convex problem of the positions of the IoT hub S and devices in the device cluster. The K-means algorithm is useful because it provides an expectation-maximization approach to solve the optimal problem. During the expectation stage, data points (i.e., latitudes and longitudes) are assigned to the closet cluster. Conveniently, the study uses a single cluster, therefore, all IoT devices have a joint cluster. Maximization is applied to exploit the centroid of the joint cluster. The K-means algorithm determines the centroid and produces the optimal problem presented in Proposition 1. Crucially, the present study investigates the UAV scheme and compares it to a terrestrial scheme. It also assumes that the TR is placed at the same position as the UAV ($lat_{TR} = lat_{U_u}$ and $long_{TR} = long_{U_u}$, however, $L_{TR}^{high} = 0$ metre while $L_{U_u}^{high} = 70$ metres) and that the TR is equipped with the same number of antennas as the UAV ($A_{TR} = A_{U_u}$) for comparative fairness.

Proposition 1: We compute the position of a UAV based on the IoT hub S and the device positions. We hypothesize that the UAV has been placed at a possible position and thereby serves all other devices in the cluster equally well. The Euclidean distances are precisely calculated on a flat earth, and the UAV's position UAV in the practical model is positioned by the K-means algorithm (Fig. 2). We note that Figure 2 contains a slight illusion. Although device D_2 is nearer to the IoT hub S than device D_1 in Cartesian coordinates, the distance of device $D_1$from the IoT hub S is less than than the distance of device D_2 on a flat earth according to Eq. (9); device D_1 is therefore the nearest device fto the IoT hub S.

Step 1: Let us assume that the IoT hub S and all terrestrial devices have a global positioning system (GPS) module. The flat earth (G2G) distances are calculated from the latitude and longitude of IoT hub S to the latitudes and longitudes of the devices and obtained as follows:

$$L_{S,D_n}^{G2G} = 2r \arctan\left(\sqrt{\Theta_{S,D_n}}, \sqrt{1-\Theta_{S,D_n}}\right), \quad (9)$$

$$\Theta_{S,D_n} = \sin\left(\frac{|lat_{D_n} - lat_S|}{360}\pi\right)^2 + \cos\left(\frac{lat_S}{180}\pi\right) \times \cos\left(\frac{lat_{D_n}}{180}\pi\right) \sin\left(\frac{|long_{D_n} - long_S|}{360}\pi\right)^2, \quad (10)$$

where $n \in N$, the latitudes and longitudes of the IoT hub S and device D_n are $(lat_S, long_S)$ and $(lat_{D_n}, long_{D_n})$, respectively, and the radius of the earth is $r = 6,378,137$ metres.

Step 2: Suppose that it is K clusters and the devices are arranged from the nearest device (denoted D_1) to the farthest device (denoted D_N), i.e., $L_{S,D_1}^{G2G} < \ldots < L_{S,D_N}^{G2G}$, for simplicity. The K-means algorithm selects the K-first devices as the centroids for the first iteration.

Step 3: The K-means algorithm computes the Euclidean distances from each data point to each centroid.

Step 4: The K-means algorithm assigns each data point (i.e., device's position) into a cluster based on the nearest distance.

Step 5: The K-means algorithm calculates the positions of K centroids according to assigned data points by using the mean function. The K-means algorithm repeats steps 3 and 4 until the assigned data points remain.

After step 5, we obtain the latitude and longitude of centroids. For simplicity, suppose that $K = 1$. In this case, the centroid is given by: The possible latitude and longitude of the FR-UAV are given, respectively, by:

$$lat_{U_u} = \frac{lat_S + lat_{D_1} + \ldots + lat_{D_N}}{N+1}, \quad (11)$$

$$long_{U_u} = \frac{long_S + long_{D_1} + \ldots + long_{D_N}}{N+1}. \quad (12)$$

Figure 2 illustrates the practical model according to positions shown in Table 2. By applying the K-means algorithm (Proposition 1), we obtain the suitable position for the TR and UAV as shown in Table 2.

C. UAV SELECTION TO ENABLE IP/EH TO PROLONG UAV LIFETIME

Although wireless communications assisted by UAVs benefit the conventional G2A, A2G or A2A links between a terrestrial IoT hub S and devices, UAVs are usually battery-operated and have limited onboard energy. The online time of an FR-UAV is limited as a consequence of the aircraft's small size and light weight. Utilization of the online time of the FR-UAV in assisting a wireless communications network is therefore a critical consideration.

TABLE 2. Positions of the IoT hub S, devices, TR and UAV.

Number of devices	$N = 3$
IoT hub S position	$lat_S = 41.16393$, $long_S = -8.58893$, $L_S^{high} = 30$ metres
D_1 position	$lat_{D_1} = 41.16129$, $long_{D_1} = -8.58485$, and $L_{D_1}^{high} = 0$ metre
D_2 position	$lat_{D_2} = 41.16258$, $long_{D_2} = -8.58258$, and $L_{D_2}^{high} = 0$ metre
D_3 position	$lat_{D_3} = 41.1625$, $long_{D_3} = -8.57839$, and $L_{D_3}^{high} = 0$ metre
Radius of the earth	$r = 6.378137 \times 10^6$ metres
Flat-earth distances (metres)	$L_{S,D_1}^{G2G} = 450.8695$, $L_{S,D_2}^{G2G} = 552.9771$, $L_{S,D_3}^{G2G} = 897.5394$, $L_{S,TR}^{G2G} = 461.1681$, $L_{TR,D_1}^{G2G} = 184.7386$, $L_{TR,D_2}^{G2G} = 93.7718$, $L_{TR,D_3}^{G2G} = 444.5217$
TR position	$lat_{TR} = 41.162700000000001$, $long_{TR} = -8.5836875$, and $L_{TR}^{high} = 0$ metre
UAV positions	$lat_{U_u} = 41.162700000000001$, $long_{U_u} = -8.5836875$, and $L_{U_u}^{high} = 70$ metres
Free space distances (metres)	$L_{S,U_u}^{A2A} = 4619264$, $L_{U_u,D_1}^{A2G} = 197.5560$, $L_{U_u,D_2}^{A2G} = 117.0177$, $L_{U_u,D_3}^{A2G} = 449.9995$
Path-loss exponent	$\varepsilon = 2$ for A2A links, $\varepsilon = 2.5$ for A2G links, and $\varepsilon = 3$ for G2G links

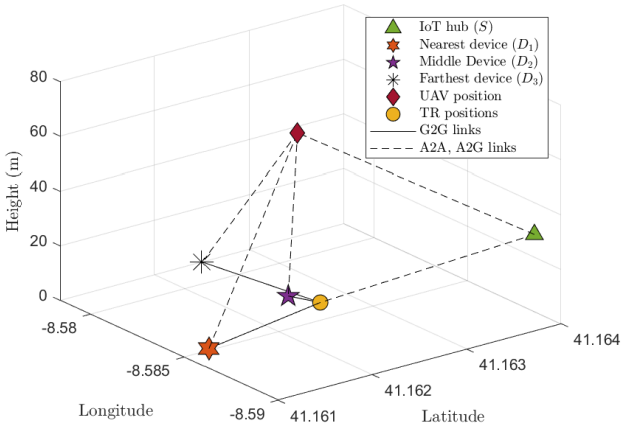

FIGURE 2. UAV/TR positioning using the K-means algorithm.

Figure 3 illustrates the power splitting scheme of the radio frequency EH enabling a pair of UAVs to assist in a MIMO-NOMA network. The scheme is different from the power splitting architectures described in other studies [33] (Fig. 4) and [47] (Fig. 4c). In [33], [47], the authors employed a single antenna at both the transmitter and receiver nodes. The authors also designed the power splitting architecture for a dual-antenna receiver [47] (Fig. 5). Inspired by these studies, we assumed that the IoT hub S, UAV and devices are equipped with antennas A_S, A_{U_u} and A_{D_n}, respectively, where $A_S \geq A_{U_u} \geq A_{D_n} \geq 2$, to improve both EH and information processing performance. Transmit antenna selection and selection combining protocols are employed at the IoT hub S and UAV, respectively. The selection combining protocol allows the UAV to select the best signal from the pre-coding matrix (1) for EH and information processing. UAV relay selection is addressed in Proposition 2.

Proposition 2: Let us assume that the UAVs U_1 and U_2 are equipped with batteries $\mathcal{B}_{U_1}$ and $\mathcal{B}_{U_2}$ (voltage). If $\mathcal{B}_{U_1} > \mathcal{B}_{U_2}$, then UAV U_1 is selected to forward the signal and UAV U_2 is placed into rest mode for radio frequency (RF)-EH to recharge its battery. However, if $\mathcal{B}_{U_1} < \mathcal{B}_{U_2}$, then UAV U_1 is switched into rest mode and UAV U_2 is switched into active mode to forward the signal. In the case of $\mathcal{B}_{U_1} = \mathcal{B}_{U_2}$, the UAV with lower indexing (i.e., U_1) is selected.

Without loss of generality and simplicity, let us assume that UAV U_1 is selected to forward the signal to devices while UAV U_2 is free in the odd transmission block $t \in \mathbf{T}^{(odd)} \subseteq 2\mathbb{N}^+ + 1$ and that UAV U_2 is selected to forward the signal to devices while UAV U_1 is free in the even transmission block $t \in \mathbf{T}^{(even)} \subseteq 2\mathbb{N}^+$, where $\mathbf{T} = \mathbf{T}^{(odd)} \cup \mathbf{T}^{(even)}$. Two stages t_1 and t_2 complete the transmission block period $t \in \mathbf{T}$, where $t = t_1 + t_2$, assuming $t_1 = t_2$.

Two simultaneous phases, t_{1a} and t_{1b}, are executed in stage t_1. In the first phase t_{1a}, the IoT hub S transmits energy for radio frequency-EH at both the selected and resting UAV by the part of the power domain in the IoT hub S by $\lambda_{U_u} P_S$, where λ_{U_u} is the power splitting factor for the UAV U_u, and P_S is the power domain at the IoT hub S. The IoT hub S simultaneously transmits superimposed messages to UAV U_1 or U_2 for data processing in the second phase t_{1b} by the remaining power domain at IoT hub S by $\left(1 - \lambda_{U_u}\right) P_S$. The UAV U_u harvests energy according to

$$E_{U_u}(t_{1a}) = \eta \lambda_{U_u} P_S \max_{[A_S \times A_{U_u}]} \left\{ \left| \mathbf{H}_{S,U_u} \right|^2 \right\}, \tag{13}$$

where $u = \{1, 2\}$ and η is the efficient EH factor.

In the second stage t_2 of transmission block period t, the selected UAV U_u (s.t. $t \in \mathbf{T}^{(odd)}$ then $u = 1$ or $t \in \mathbf{T}^{(even)}$ then $u = 2$) forwards the superimposed signal to devices with power domain P_{U_u} while the resting UAV harvests energy from the IoT hub S with power domain P_S. After the second stage of transmission block period t, the resting UAV $U_{\bar{u}}$ harvests energy according to

$$E_{U_{\bar{u}}}(t_2) = \eta \left(P_S \max_{[A_S \times A_{U_{\bar{u}}}]} \left\{ \left| \mathbf{H}_{S,U_{\bar{u}}} \right|^2 \right\} \right). \tag{14}$$

Proposition 3: EH at the resting UAV $U_{\bar{u}}$ during a single transmission block period t is expressed as

$$E_{U_{\bar{u}}}(t) = \eta \left(\left(1 + \lambda_{U_{\bar{u}}}\right) P_S \sigma_{S,U_{\bar{u}}} \right), \tag{15}$$

where the expected channel gain $\sigma_{S,U_{\bar{u}}} = E\left\{ \left| \mathbf{H}_{S,U_{\bar{u}}} \right|^2 \right\}$.

The coupled aerial relays are switchable, which allows the IoT hub S to select the UAV U_1 or U_2 to forward the signal in different transmission blocks. In this manner, the FR-UAV's online time is prolonged.

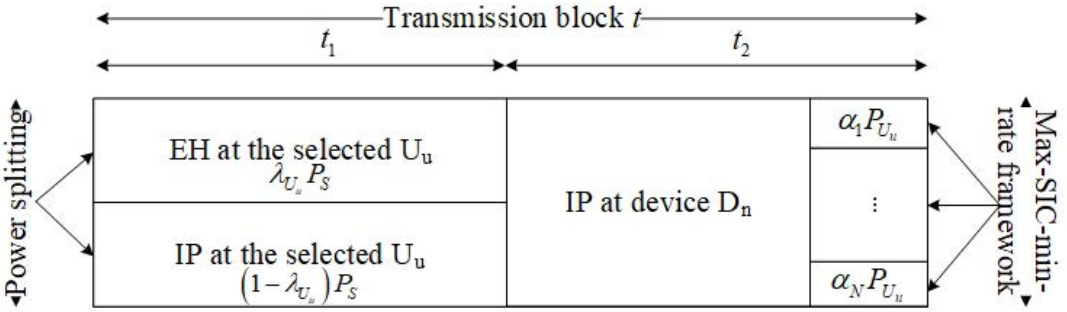

FIGURE 3. EH and information processing (IP) at the selected UAV U_u during a transmission block period $t \in \left\{\mathbf{T}^{(odd)}, \mathbf{T}^{(even)}\right\} \subseteq \mathbf{T}$.

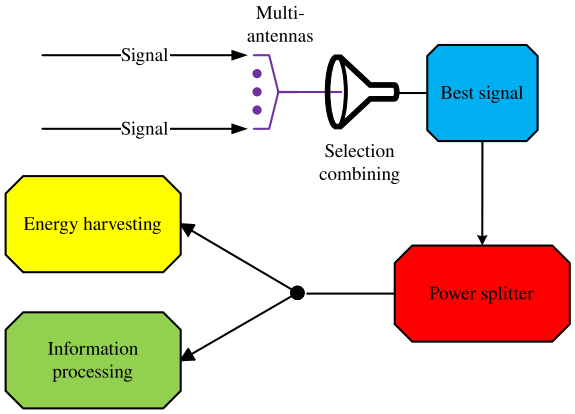

FIGURE 4. Scheme illustrating the selection combining and power splitting architecture for a UAV-assisted MIMO-NOMA wireless communications network.

D. INFORMATION PROCESSING AND FORMULATIONS

Figure 4 depicts an architecture which combines the transmit antenna selection/selection combining technique and the power splitting protocol to assist EH and information processing at the selected UAV U_u.

The IoT hub S encodes the messages $\mathbf{X} = \{x_1, \ldots, x_N\}$ of the terminal devices and superimposes the messages into the signal by sharing the remaining power domain $(1 - \lambda_{U_u})P_S$ using different PA factors $\mathbf{W} = \{\alpha_1, \ldots, \alpha_N\}$. From the pre-coding matrix $\mathbf{H}_{S,U_u}$, as shown by (1), only the best channel is selected for signal transmission. In the second phase $t_{1b} \in t_1 \in t \in \mathbf{T}$, the selected UAV U_u receives a radio frequency signal according to the equation

$$y_{U_u}(t_{1b}) = \sqrt{(1-\lambda_{U_u}) P_S} \max_{[A_S \times A_{U_u}]} \left\{ \left| \mathbf{H}_{S,U_u} \right| \right\} \times \sum \left(\sqrt{\mathbf{W}} \times \mathbf{X} \right) + n_{U_u}, \quad (16)$$

$$init : \bar{\mathbf{X}} \leftarrow \mathbf{X},\ \hat{\mathbf{X}} \leftarrow \emptyset,\ \bar{\mathbf{W}} \leftarrow \mathbf{W},\ \hat{\mathbf{W}} \leftarrow \emptyset, \quad (17)$$

where the selected UAV $U_u = U_1$ if $t_{1b} \in \mathbf{T}^{(odd)}$ transmission block or $U_u = U_2$ if $t_{1b} \in \mathbf{T}^{(even)}$ transmission block, and n_{U_u} is the additive white Gaussian noise (AWGN), i.e., $n_{U_u} \sim \mathcal{CN}(0, N_0)$ with zero mean and N_0 variance, at the selected UAV U_u. We assume $E\left\{|x_1|^2\right\} = \ldots = E\left\{|x_1|^2\right\} = 1$.

Proposition 4: Applying max-SIC, the SINR at the selected UAV U_u if U_u decodes the best message $\exists x_i \in \bar{\mathbf{X}}$, which has the best power allocation factor $\max\left\{\bar{\mathbf{W}}\right\}$, and treating other messages $\forall x_j \in \bar{\mathbf{X}} \backslash x_i$ and AWGN n_{U_u} as interference, is expressed as

$$\gamma_{U_u - x_i}(t_{1b}) = \frac{\left(1-\lambda_{U_u}\right) \max\limits_{[A_S \times A_{U_u}]} \left\{ \left| \mathbf{H}_{S,U_u} \right|^2 \right\} \max\left\{\bar{\mathbf{W}}\right\} \rho_S}{\left(1-\lambda_{U_u}\right) \max\limits_{[A_S \times A_{U_u}]} \left\{ \left| \mathbf{H}_{S,U_u} \right|^2 \right\} \rho_S \sum \bar{\mathbf{W}} \backslash \alpha_i + 1}, \quad (18)$$

$$while : \bar{\mathbf{W}} \neq \emptyset \text{ and } \bar{\mathbf{X}} \neq \emptyset \quad (19)$$

$$s.t. : x_i = \max\left\{\bar{\mathbf{X}}\right\} \text{ and } \alpha_i = \max\left\{\bar{\mathbf{W}}\right\}, \quad (20)$$

$$update : \bar{\mathbf{X}} \leftarrow \bar{\mathbf{X}} \backslash x_i, \hat{\mathbf{X}} \leftarrow \hat{\mathbf{X}} \cup x_i, \bar{\mathbf{W}} \leftarrow \bar{\mathbf{W}} \backslash \alpha_i \text{ and } \hat{\mathbf{W}} \leftarrow \hat{\mathbf{W}} \cup \alpha_i, \quad (21)$$

where the signal to noise ratio (SNR) $\rho_S = \frac{P_S}{N_0}$, $\bar{\mathbf{X}}$ is the set of non-decoded messages and $\bar{\mathbf{W}}$ is the set of power allocation factors of non-decoded messages. $\bar{\mathbf{W}}$ and $\bar{\mathbf{X}}$ in (19) are given by (17). When the best message $x_i = \max\left\{\bar{\mathbf{X}}\right\}$ with maximum power allocation factor $(\alpha_i = \max\left\{\bar{\mathbf{W}}\right\})$ is selected, then the best message x_i is decoded according to (18) by treating other messages $\bar{\mathbf{X}} \backslash x_i$ and AWGN n_{U_u} as interference. After the best message x_i is decoded, we update $\bar{\mathbf{X}} \leftarrow \bar{\mathbf{X}} \backslash x_i$, $\hat{\mathbf{X}} \leftarrow \hat{\mathbf{X}} \cup x_i$, $\bar{\mathbf{W}} \leftarrow \bar{\mathbf{W}} \backslash \alpha_i$ and $\hat{\mathbf{W}} \leftarrow \hat{\mathbf{W}} \cup \alpha_i$. Equation (18) is repeated until only one message remains. The final message is decoded by treating AWGN n_{U_u} as interference according to the equation

$$\gamma_{U_u - x_i}(t_{1b}) = \left(1-\lambda_{U_u}\right) \max_{[A_S \times A_{U_u}]} \left\{ \left| \mathbf{H}_{S,U_u} \right|^2 \right\} \min\{\mathbf{W}\} \rho_S. \quad (22)$$

After decoding the final message, we obtain $\bar{\mathbf{X}} \leftarrow \bar{\mathbf{X}} \backslash x_i = \emptyset$, $\hat{\mathbf{X}} \leftarrow \hat{\mathbf{X}} \cup x_i = \mathbf{X}$, $\bar{\mathbf{W}} \leftarrow \bar{\mathbf{W}} \backslash \alpha_i = \emptyset$ and $\hat{\mathbf{W}} \leftarrow \hat{\mathbf{W}} \cup \alpha_i = \mathbf{W}$. Since $\bar{\mathbf{X}} = \emptyset$, all messages in the received signal (16) have been decoded.

The maximum instantaneous bit-rate threshold attained if the selected UAV U_u decodes message x_i in the best received

signal according to (16) is expressed as

$$\max_{[A_S \times A_{U_u}]} \left\{ R_{U_u - x_i}(t_{1b}) \right\} = \frac{1}{2}\log_2 \left(1 + \max_{[A_S \times A_{U_u}]} \left\{ \gamma_{U_u - x_i}(t_{1b}) \right\} \right). \quad (23)$$

The minimum-maximum instantaneous bit-rate threshold attained when the selected UAV U_u decodes message $\forall x_i \in \bar{\mathbf{W}}$ in the best received signal according to (16) is expressed as:

$$\min_{\forall x_i \in \mathbf{X}} \max_{[A_S \times A_{U_u}]} \left\{ R_{U_u - x_i}(t_{1b}) \right\} = \frac{1}{2}\log_2 \left(1 + \min_{\forall x_i \in \mathbf{X}} \max_{[A_S \times A_{U_u}]} \left\{ \gamma_{U_u - x_i}(t_{1b}) \right\} \right). \quad (24)$$

In the second stage $t_2 \in t \in \mathbf{T}$, the selected UAV U_u retrieves, re-encodes and forwards the superimposed signal to the devices. There are two major forwarding protocols: amplify-and-forward and decode-and-forward. In a previous study, it was verified that the amplify-and-forward protocol obtains superior performance to decode-and-forward in individual schemes [48]. In [49], it was verified that amplify-and-forward cannot be employed at a relay because relays have insufficient energy. Similarly, the aerial relays depicted in Figure 1 have limited energy. The present study therefore applies the decode-and-forward protocol to ensure the aerial relay successfully receives and decodes messages. This study also employed Transmit antenna selection at the UAV and selection combining protocols at devices are also used to select the best signal in the pre-coding matrix according to Eq. (3). The best-received signal at terminal device D_n is expressed as

$$y_{D_n}(t_2) = \max_{[A_{U_u} \times A_{D_n}]} \left\{ \left| \mathbf{H}_{U_u, D_n} \right| \right\} \sqrt{P_{U_u}} \sum \left(\sqrt{\mathbf{W}} \times \mathbf{X} \right) + n_{D_n}, \quad (25)$$

$$init : \bar{\mathbf{X}} \leftarrow \mathbf{X},\ \hat{\mathbf{X}} \leftarrow \emptyset,\ \bar{\mathbf{W}} \leftarrow \mathbf{W},\ \hat{\mathbf{W}} \leftarrow \emptyset, \quad (26)$$

where P_{U_u} is the power domain at the selected UAV U_u and n_{D_n} is AWGN at device D_n, i.e. $n_{D_n} \sim \mathcal{CN}(0, N_0)$, assuming $P_{U_1} = P_{U_2}$ for simplicity.

Device D_n also employs max-SIC to decode its own message x_n. If the device D_n decodes the data symbol x_i, the SINR obtained at device D_n is expressed as

$$\gamma_{D_n - x_i}(t_2) = \frac{\max_{[A_{U_u} \times A_{D_n}]} \left\{ \left| \mathbf{H}_{U_u, D_n} \right|^2 \right\} \alpha_i \rho_{U_u}}{\max_{[A_{U_u} \times A_{D_n}]} \left\{ \left| \mathbf{H}_{U_u, D_n} \right|^2 \right\} \rho_{U_u} \sum \bar{\mathbf{W}} \backslash \alpha_i + 1}, \quad (27)$$

$$while : \bar{\mathbf{W}} \neq \emptyset \text{ and } \bar{\mathbf{X}} \neq \emptyset \quad (28)$$

$$find : x_i = \max \left\{ \bar{\mathbf{X}} \right\} \text{ and } \alpha_i = \max \left\{ \bar{\mathbf{W}} \right\}, \quad (29)$$

$$update : \bar{\mathbf{X}} \leftarrow \bar{\mathbf{X}} \backslash x_i, \hat{\mathbf{X}} \leftarrow \hat{\mathbf{X}} \cup x_i,$$

$$\bar{\mathbf{W}} \leftarrow \bar{\mathbf{W}} \backslash \alpha_i \text{ and } \hat{\mathbf{W}} \leftarrow \hat{\mathbf{W}} \cup \alpha_i \quad (30)$$

$$break : \text{ if } i = n, \quad (31)$$

where SNR $\rho_{U_u} = \frac{P_{U_u}}{N_0}$ in dB, $\bar{\mathbf{W}}$ and $\bar{\mathbf{X}}$ in (28) are given by (26). Device D_n repeats max-SIC according to (27) while $i \neq n$. This means that D_n's message x_n has not yet been decoded.

The maximum of the instantaneous bit-rate threshold attained when the terminal device D_n in the second stage $t_2 \in \mathbf{T}$ decodes the data symbols x_i in the best received signal according to (25) is expressed as

$$\max_{[A_{U_u} \times A_{D_n}]} \left\{ R_{D_n - x_i}(t_2) \right\}_{\forall x_i \geq x_n} = \frac{1}{2}\log_2 \left(1 + \max_{[A_{U_u} \times A_{D_n}]} \left\{ \gamma_{D_n - x_i}(t_2) \right\}_{\forall x_i \geq x_n} \right). \quad (32)$$

The minimum of the maximal-instantaneous bit-rate threshold attained at device D_n when it decodes messages $\forall x_i \geq x_n$ is expressed as

$$\min_{\forall x_i \geq x_n} \max_{[A_{U_u} \times A_{D_n}]} \left\{ R_{D_n - x_i}(t) \right\} = \frac{1}{2}\log_2 \left(1 + \min_{\forall x_i \geq x_n} \max_{[A_{U_u} \times A_{D_n}]} \left\{ \gamma_{D_n - x_i}(t) \right\} \right). \quad (33)$$

III. SYSTEM PERFORMANCE ANALYSIS

In [49] and [50], the application of a max-SIC-min-rate framework is described. The present study proposes the application of Algorithms 1 and 2 to the max-SIC-min-rate framework and investigating the outage probability at the UAV and terminal devices. Novel closed-form expressions of the outage probability at the selected UAV U_u and device D_n for both independent propagation scenarios $Q = \{(i), (ii)\}$ are also derived, where (i) two-stage Rayleigh fading channels and (ii) two-stage Nakagami-m fading channels.

A. DESIGN FOR A MAX-SIC-MIN-RATE FRAMEWORK

In a previous study, the authors assumed that devices are arranged from the nearest device D_1 to the farthest device D_N [50], [51], or for simplicity, from the nearest device D_N to the farthest device D_1 [52]. Therefore, the power allocation factors described in [50] and [51] followed the arrangement $\alpha_1 < \ldots < \alpha_N$ or $\alpha_1 > \ldots > \alpha_N$, as in [52]. By applying conventional SIC, the authors sequentially decoded messages $x_N \rightarrow x_1$ as in [50] and [51] or $x_1 \rightarrow x_N$ as in [52]. By contrast, the devices were non-ordered after UAV positioning, therefore, conventional SIC cannot be applied to decode the messages. The present study proposes a max-SIC-min-rate framework to solve this problem. From the equation for the best received signal (16), max-SIC (18) and min-rate (24), we introduce the information processing architecture at the UAV:

- *Step 1*: The selected UAV U_u receives the superimposed signal according to (16);

- *Step 2*: By using transmit antenna selection and the selection combining technique, the selected UAV U_u obtains the SINR from the best selected antenna according to (18) and (22). If message x_i, i.e., $x_i = \max\{\bar{\mathbf{X}}\}$, is decoded, $\bar{\mathbf{X}} \leftarrow \bar{\mathbf{X}} \backslash x_i, \hat{\mathbf{X}} \leftarrow \hat{\mathbf{X}} \cup x_i, \bar{\mathbf{W}} \leftarrow \bar{\mathbf{W}} \backslash \alpha_i$ and $\hat{\mathbf{W}} \leftarrow \hat{\mathbf{W}} \cup \alpha_i$ is updated;
- *Step 3*: The selected UAV U_u obtains the instantaneous bit-rate threshold according to (23). If (19) is true, max-SIC-min-rate framework repeats Step 2, otherwise max-SIC-min-rate framework proceeds to Step 4;
- *Step 4*: The selected UAV determines the minimum instantaneous bit-rate threshold according to (24);
- *Step 5*: The selected UAV compares the minimum instantaneous bit-rate threshold given by (24) to the bit-rate threshold $\mathcal{R}$ (bps/Hz) at the devices. Two cases are possible: in the first case, if the minimum instantaneous bit-rate threshold is less than the pre-defined bit-rate threshold $\mathcal{R}$ at the devices, an outage event occurs at the selected UAV U_u; in the second case, if the minimum of instantaneous bit-rate thresholds according to (24) reaches the bit-rate threshold $\mathcal{R}$ at the devices, the other instantaneous bit-rate thresholds given by (23) consequently also attain the device bit-rate threshold $\mathcal{R}$. In other words, the selected UAV decodes all messages successfully. The selected UAV U_u then re-encodes and forwards the superimposed signal to the devices.

The information processing architecture at the device $D_n = \{D_1, \ldots, D_N\}$ is also introduced.

- *Step 1*: Device $D_n = \{D_1, \ldots, D_N\}$ receives the superimposed signal from the selected UAV U_u according to (25);
- *Step 2*: By using transmit antenna selection/selection combining techniques and max-SIC, device D_n obtains the SINR according to (27). If message x_i ($x_i = \max\{\bar{\mathbf{X}}\}$) is decoded, $\bar{\mathbf{X}} \leftarrow \bar{\mathbf{X}} \backslash x_i, \hat{\mathbf{X}} \leftarrow \hat{\mathbf{X}} \cup x_i, \bar{\mathbf{W}} \leftarrow \bar{\mathbf{W}} \backslash \alpha_i$ and $\hat{\mathbf{W}} \leftarrow \hat{\mathbf{W}} \cup \alpha_i$ is updated;
- *Step 3*: Device D_n obtains the instantaneous bit-rate threshold according to (32). Device D_n repeats *Step 2* while $i \neq n$. If $i = n$, then Step 4 is executed;
- *Step 4*: Device D_n calculates the minimum of instantaneous bit-rate thresholds as shown in (33);
- *Step 5*: Device D_n compares the minimum instantaneous bit-rate threshold according to (33) to the bit rate threshold $\mathcal{R}$ of devices. Two cases are possible: in the first case, if the minimum instantaneous bit-rate threshold according to (33) is less than the bit-rate threshold $\mathcal{R}$ at the devices, an outage event occurs at device D_n; in the second case, if the minimum of instantaneous bit rate threshold according to (33) attains the bit rate threshold $\mathcal{R}$ at the devices, the other instantaneous bit rate thresholds consequently also attain the bit rate threshold $\mathcal{R}$ of devices. Message x_n is thus propagated to device D_n successfully.

B. OUTAGE PROBABILITY PERFORMANCE

Theorem 1: The outage event at the selected UAV U_u occurs if the minimum instantaneous bit-rate thresholds according to (24) cannot attain the pre-defined bit-rate threshold $\mathcal{R}$ (bps/Hz). Therefore, the outage probability at the selected UAV U_u in transmission block t in scenario $Q = \{(i), (ii)\}$ is expressed as

$$OP_{U_u}^{Q}(t) = 1 - \Pr\left\{\min_{\forall x_i \in \bar{\mathbf{X}}} \max_{[A_S \times A_{U_u}]} \left\{R_{U_u - x_i}(t)\right\} \geq \mathcal{R}\right\}. \tag{34}$$

To apply (34), we propose Algorithm 1 to obtain the Monte Carlo simulations of the outage probability at the selected UAV U_u.

Algorithm 1 Adopt a Max-SIC-Min-Rate Framework to Determine the Outage Probability at the Selected UAV U_u According to (34) for Transmission Block t and Scenario $Q = \{(i), (ii)\}$

Input: Initialize parameters in Tables 2 and 4. Randomly generate 10^6 samples of each fading channel over Rayleigh or Nakagami-m distribution

Output: Simulated (Sim) results for outage probability at the selected UAV U_u for transmission block t and scenario Q

```
Select the best received signal according to (16)
while (W̄ ≠ ∅ and X̄ ≠ ∅) do
    Find x_i = max{X̄} and α_i = max{W̄}
    Calculate SINR according to (18) or (22)
    Calculate the achievable instantaneous bit-rate according to (23);
    Update X̄ ← X̄\x_i, X̂ ← X̂ ∪ x_i, W̄ ← W̄\α_i and Ŵ ← Ŵ ∪ α_i
end while
Find the minimum instantaneous bit-rate threshold according to (24)
Initialize variable count ← 0;
for l = 1 to 10^6 samples do
    if ( min_{∀x_i∈X̄} max_{[A_S×A_{U_u}]} {R_{U_u−x_i}(t)} ≥ R ) then
        count ← count + +
    end if
end for
return OP at selected UAV as given by OP^Q_{U_u}(t) = 1 − count / 10^6
```

Theorem 2: The outage event at terminal device D_n for $n \leq N$ occurs when FR-UAV cannot decode at least a message in $\mathbf{X}$ from the best received signal $y_{U_u}(t)$ according to (16) or the terminal device D_n cannot decode at least a message in $\bar{\mathbf{X}}$ from the best received signal $y_{D_n}(t)$ according to (25). Therefore, the outage probability at terminal device D_n underlying the U_u-assisted MIMO-NOMA network is

expressed as

$$OP_{D_n}^{Q}(t) = 1 - \Pr\left\{ \min_{\forall x_i \geq x_n} \max_{[A_S \times A_{U_u}]} \left\{ R_{U_u - x_i}(t) \right\} \geq \mathcal{R}, \min_{\forall x_i \geq x_n} \max_{[A_{U_u} \times A_{D_n}]} \left\{ R_{D_n - x_i}(t) \right\} \geq \mathcal{R} \right\}. \quad (35)$$

Combining (35) and the information processing architecture at device D_n, Algorithm 2 produces the Monte Carlo simulations of the outage probability at device D_n for transmission block t and scenario Q.

Algorithm 2 Adopt a Max-SIC-Min-Rate Framework to Determine the Outage Probability at Terminal Device D_n According to (35) for Transmission Block t and Scenario $Q = \{(i), (ii)\}$

Input: Initialize parameters in Tables 2 and 4. Randomly generate 10^6 samples of each fading channel over Rayleigh or Nakagami-m distribution

Output: Simulated (Sim) results for outage probability at device D_n

Select the best received signals according to (16) and (25)
while $\left(\bar{\mathbf{W}} \neq \emptyset \text{ and } \bar{\mathbf{X}} \neq \emptyset\right)$ **do**
  Find $x_i = \max\left\{\bar{\mathbf{X}}\right\}$ and $\alpha_i = \max\left\{\bar{\mathbf{W}}\right\}$
  Calculate SINR at the selected UAV U_u according to (18) or (22)
  Calculate the achievable instantaneous bit-rate at the selected UAV U_u according to (23)
  Calculate SINR at the device D_n according to (27)
  Calculate the achievable instantaneous bit-rate at device D_n according to (32)
  Update $\bar{\mathbf{X}} \leftarrow \bar{\mathbf{X}} \backslash x_i, \hat{\mathbf{X}} \leftarrow \hat{\mathbf{X}} \cup x_i, \bar{\mathbf{W}} \leftarrow \bar{\mathbf{W}} \backslash \alpha_i$ and $\hat{\mathbf{W}} \leftarrow \hat{\mathbf{W}} \cup \alpha_i$
  if $(i == n)$ **then**
    Break
  end if
end while
Find the minimum instantaneous bit-rate threshold at the selected UAV U_u according to (24)
Find the minimum instantaneous bit-rate threshold at device D_n according to (33)
Initialize variable $count \leftarrow 0$
for $l = 1$ to 10^6 samples **do**
  if $\left(\min\left\{ \min_{\forall x_i \geq x_n} \max_{[A_S \times A_{U_u}]} \left\{ R_{U_u - x_i}(t) \right\}, \min_{\forall x_i \geq x_n} \max_{[A_{U_u} \times A_{D_n}]} \left\{ R_{D_n - x_i}(t) \right\} \right\} \geq \mathcal{R} \right)$ **then**
    $count \leftarrow count + +$
  end if
end for
return OP at device D_n as given by $OP_{D_n}^{Q}(t) = 1 - count \,/ 10^6$

1) PROPAGATION OVER TWO-STAGE RAYLEIGH AND RAYLEIGH FADING CHANNELS

In scenario (i), fading channels are distributed over Rayleigh fading channels for both stages of transmission block t.

Remark 1: The outage probability at the selected UAV U_u in transmission block t and scenario $Q = (i)$ is obtained from (34) in Theorem 1 and expressed in novel closed-form as

$$OP_{U_u}^{(i)}(t) = \sum_{\psi=0}^{A_S A_{U_u}} \frac{(-1)^{\psi} \left(A_S A_{U_u}\right)!}{\psi! \left(A_S A_{U_u} - \psi\right)!} \times \exp\left(- \frac{\psi \gamma}{\left(1 - \lambda_{U_u}\right) \beta \rho_S \sigma_{S,U_u}} \right), \quad (36)$$

$$\text{s.t.} \quad \beta_i = \alpha_i - \gamma \sum \left(\bar{\mathbf{W}} \backslash \alpha_i \right), \quad (37)$$

$$\beta = \min\left\{\beta_i\right\}, \quad (38)$$

where α_i in (37) is given by (21) and SINR threshold $\gamma = 2^{2\mathcal{R}} - 1$. See Appendix A for proof.

Remark 2: The outage probability at device D_n is obtained from (35) for transmission block t and scenario $Q = (i)$, where the fading channels from the IoT hub S to the selected UAV U_u and from U_u to the devices are distributed over two-stage Rayleigh fading channels. Applying PDF according to (5), we derive the outage probability at device D_n for $n \in N$ and express it in closed-form as

$$OP_{D_n}^{(i)}(t) = \sum_{\psi=0}^{A} \frac{(-1)^{\psi} A!}{\psi! (A - \psi)!} \exp\left(- \frac{\psi \gamma}{\Omega_n} \right), \quad (39)$$

$$\text{s.t.} \ \varpi_n = \min\left\{ \left(1 - \lambda_{U_u}\right) \beta_i \rho_S \sigma_{S,U_u} \right\}, \quad (40)$$

$$\omega_n = \min\left\{ \beta_i \rho_{U_u} \sigma_{U_u,D_n} \right\}, \quad (41)$$

$$\Omega_n = \min\left\{\varpi_n, \omega_n\right\}, \quad (42)$$

$$A = \begin{cases} A_S A_{U_u} \text{ for } \Omega_n = \varpi_n, \\ A_{U_u} A_{D_n} \text{ for } \Omega_n = \omega_n, \end{cases} \quad (43)$$

where β_i in (40) and (41) are obtained from (37). See Appendix B for proof.

Corollary 1: According to expression (23) in [49], expressions (35) is rewritten as

$$OP_{D_n}^{(i)} = \Pr\left\{ \min_{\forall x_i \geq x_n} \max_{[A_S \times A_{U_u}]} \left\{ R_{U_u - x_i}^{(i)} < \mathcal{R} \right\} \right\} + \Pr\left\{ \min_{\forall x_i \geq x_n} \max_{[A_S \times A_{U_u}]} \left\{ R_{U_u - x_i}^{(i)} \geq \mathcal{R} \right\}, \min_{\forall x_i \geq x_n} \max_{[A_{U_u} \times A_{D_n}]} \left\{ R_{D_n - x_i}^{(i)} < \mathcal{R} \right\} \right\}. \quad (44)$$

Let $OP_{U_u - x_i}^{(i)} = \Pr\left\{ \min_{\forall x_i \geq x_n} \max_{[A_S \times A_{U_u}]} \left\{ R_{U_u - x_i}^{(i)} < \mathcal{R} \right\} \right\}$ and $OP_{D_n - x_i}^{(i)} = \Pr\left\{ \min_{\forall x_i \geq x_n} \max_{[A_{U_u} \times A_{D_n}]} \left\{ R_{D_n - x_i}^{(i)} < \mathcal{R} \right\} \right\}$. According to expression (24) in [49], expression (44) is derived and

obtained in closed form according to MIMO scheme as

$$OP_{D_n}^{(i)} = \left[OP_{U_u-x_i}^{(i)} + \left[\left(1 - OP_{U_u-x_i}^{(i)}\right) - \left(1 - OP_{D_n-x_i}^{(i)}\right) \right]^+ \right]^+, \tag{45}$$

where $OP_{U_u-x_i}^{(i)}$ and $OP_{D_n-x_i}^{(i)}$ are given by (46) and (47), respectively.

$$OP_{U_u-x_i}^{(i)} = \sum_{\psi=0}^{A_S A_{U_u}} \frac{(-1)^{\psi} \left(A_S A_{U_u}\right)!}{\psi! \left(A_S A_{U_u} - \psi\right)!} \exp\left(-\frac{\psi\gamma}{\varpi_n}\right), \tag{46}$$

$$OP_{D_n-x_i}^{(i)} = \sum_{\psi=0}^{A_{U_u} A_{D_n}} \frac{(-1)^{\psi} \left(A_{U_u} A_{D_n}\right)!}{\psi! \left(A_{U_u} A_{D_n} - \psi\right)!} \exp\left(-\frac{\psi\gamma}{\omega_n}\right), \tag{47}$$

where ϖ_n in (46) and ω_n in (47) are given by (40) and (41), respectively, and β_i in (40) and (41) is given by (37).

2) PROPAGATION OVER NAKAGAMI-*m* AND NAKAGAMI-*m* FADING CHANNELS

In scenario (*ii*), propagation is distributed over Nakagami-*m* fading channels for both stages in transmission block t.

Remark 3: The outage probability at the selected UAV U_u is obtained from (34) in Theorem 2, and the CDF is obtained from (8). We therefore derive the closed-form expression for the outage probability at the selected UAV U_u for transmission block t and scenario (*ii*) as follows:

$$OP_{U_u}^{(ii)}(t) = \prod_{a=1}^{A_S} \prod_{b=1}^{A_{U_u}} \left(1 - \exp\left(-\frac{m\gamma}{\left(1-\lambda_{U_u}\right)\beta\rho_S\sigma_{S,U_u}}\right) \times \sum_{\eta=0}^{m-1} \frac{1}{\eta!} \left(\frac{m\gamma}{\left(1-\lambda_{U_u}\right)\beta\rho_S\sigma_{S,U_u}}\right)^{\eta}\right), \tag{48}$$

where β in expression (48) is obtained from (38). See Appendix C for proof.

Remark 4: From (35) and CDF (8), we derive the outage probability in closed-form at device D_n for $n \in N$ as follows:

$$OP_{D_n}^{(ii)}(t) = \prod_{\psi=1}^{A} \left(1 - \exp\left(-\frac{m\gamma}{\Omega_n}\right) \sum_{\eta=0}^{m-1} \frac{1}{\eta!} \left(\frac{m\gamma}{\Omega_n}\right)^{\eta}\right), \tag{49}$$

where Ω_n and factor A are obtained from (42) and (43), respectively. See Appendix D for proof.

Corollary 2: According to Corollary 1, outage probability of device D_n in scheme (*ii*) is rewritten as

$$OP_{D_n}^{(ii)} = \Pr\left\{ \min_{\forall x_i \geq x_n} \max_{[A_S \times A_{U_u}]} \left\{ R_{U_u-x_i}^{(ii)} < \mathcal{R} \right\} \right\} + \Pr\left\{ \min_{\forall x_i \geq x_n} \max_{[A_S \times A_{U_u}]} \left\{ R_{U_u-x_i}^{(ii)} \geq \mathcal{R} \right\}, \min_{\forall x_i \geq x_n} \max_{[A_{U_u} \times A_{D_n}]} \left\{ R_{D_n-x_i}^{(ii)} < \mathcal{R} \right\} \right\}. \tag{50}$$

Let $OP_{U_u-x_i}^{(ii)} = \Pr\left\{ \min_{\forall x_i \geq x_n} \max_{[A_S \times A_{U_u}]} \left\{ R_{U_u-x_i}^{(ii)} < R \right\} \right\}$ and $OP_{D_n-x_i}^{(ii)} = \Pr\left\{ \min_{\forall x_i \geq x_n} \max_{[A_{U_u} \times A_{D_n}]} \left\{ R_{D_n-x_i}^{(ii)} < R \right\} \right\}$. Expression (50) is derived and obtained in closed form according to the MIMO over Nakagami-*m* scheme as

$$OP_{D_n}^{(ii)} = \left[OP_{U_u-x_i}^{(ii)} + \left[\left(1 - OP_{U_u-x_i}^{(ii)}\right) - \left(1 - OP_{D_n-x_i}^{(ii)}\right) \right]^+ \right]^+, \tag{51}$$

where $OP_{U_u-x_i}^{(ii)}$ and $OP_{D_n-x_i}^{(ii)}$ are given by (50) and (53), respectively.

$$OP_{U_u-x_i}^{(ii)} = \prod_{a=1}^{A_S} \prod_{b=1}^{A_{U_u}} \left(1 - \exp\left(-\frac{m\gamma}{\left(1-\lambda_{U_u}\right)\beta_i\rho_S\sigma_{S,U_u}}\right) \times \sum_{\eta=0}^{m-1} \frac{1}{\eta!} \left(\frac{m\gamma}{\left(1-\lambda_{U_u}\right)\beta_i\rho_S\sigma_{S,U_u}}\right)^{\eta}\right), \tag{52}$$

$$OP_{D_n-x_i}^{(ii)} = \prod_{b=1}^{A_{U_u}} \prod_{c=1}^{A_{D_n}} \left(1 - \exp\left(-\frac{m\gamma}{\beta_i\rho_{U_u}\sigma_{U_u,D_n}}\right) \times \sum_{\eta=0}^{m-1} \frac{1}{\eta!} \left(\frac{m\gamma}{\beta_i\rho_{U_u}\sigma_{U_u,D_n}}\right)^{\eta}\right), \tag{53}$$

where β_i in (52) and (53) is given by (37).

IV. NUMERICAL RESULTS

Assuming the existence of three IoT devices in the NOMA-IoT cluster (Table 2) and applying (9), the flat earth distances L_{S,D_n}^{G2G} from the IoT hub S are calculated. We obtained $L_{S,D_1}^{G2G} < L_{S,D_2}^{G2G} < L_{S,D_3}^{G2G}$ as shown in Table 2, and verified the G2G distances using the Google Maps tool. The latitudinal and longitudinal positions of the centroid where FR/TR are positioned (i.e., yellow-circle in Fig. 2) are given by the K-means algorithm according to Proposition 1. After positioning the FR/TR, we obtained $L_{TR,D_2}^{G2G} < L_{TR,D_1}^{G2G} < L_{TR,D_3}^{G2G}$ and $L_{U_u,D_2}^{A2G} < L_{U_u,D_1}^{A2G} < L_{U_u,D_3}^{A2G}$. The power allocation factors are $\alpha_1 = 0.3333$, $\alpha_2 = 0.1667$ and $\alpha_3 = 0.5$. For simplicity, we assume that the transmit powers at the IoT hub S and TR are $\rho_S = \rho_{TR}$ in dB, while the transmit power at the UAVs U_1 and U_2 are $\rho_{U_1} = \rho_{U_2} = \frac{1}{5}\rho_S$ in dB. Tables 2 and 4 describe in detail the parameters that were applied for analysis (ana) and the Monte Carlo simulations (sim). The following sections present an analysis and the simulation results for a UAV compared to a TR-assisted NOMA-IoT network for the twelve independent models as shown in Table 3.

A. DISCUSSION OF MODELS 1 AND 2

Figure 5 plots the outage probability of a SISO-IoT network by equipping antennas at the IoT hub S, UAV U_u and TR, and devices with $A_S = 1$, $A_{U_u} = A_{TR} = 1$, and $A_{D_n} = 1$, respectively. A comparison of the results in Figures 5a, 5b, 5c and 5d indicates that the FR-IoT network provides strongly better system performance than TR-IoT network. As proof,

TABLE 3. Description of investigation models.

	TR	FR	Number of antennas	Rayleigh	Nakagami-m	Figures
Model 1	•		SISO with $A_S = A_{TR} = A_{D_n} = 1$	•		Figure 5
Model 2		•	SISO with $A_S = A_{U_u} = A_{D_n} = 1$	•		
Model 3	•		SISO with $A_S = A_{TR} = A_{D_n} = 1$		• with $m = 3$	Figure 6
Model 4		•	SISO with $A_S = A_{U_u} = A_{D_n} = 1$		• with $m = 3$	
Model 5	•		MIMO with $A_S = A_{TR} = 4, A_{D_n} = 2$	•		Figure 7
Model 6		•	MIMO with $A_S = A_{U_u} = 4, A_{D_n} = 2$	•		
Model 7	•		MIMO with $A_S = A_{TR} = 4, A_{D_n} = 2$		• with $m = 3$	Figure 8
Model 8		•	MIMO with $A_S = A_{U_u} = 4, A_{D_n} = 2$		• with $m = 3$	
Model 9	•		mMIMO with $A_S = 128, A_{TR} = 4, A_{D_n} = 2$	•		Figure 9
Model 10		•	mMIMO with $A_S = 128, A_{U_u} = 4, A_{D_n} = 2$	•		
Model 11	•		mMIMO with $A_S = 128, A_{TR} = 4, A_{D_n} = 2$		• with $m = 3$	Figure 10
Model 12		•	mMIMO with $A_S = 128, A_{U_u} = 4, A_{D_n} = 2$		• with $m = 3$	

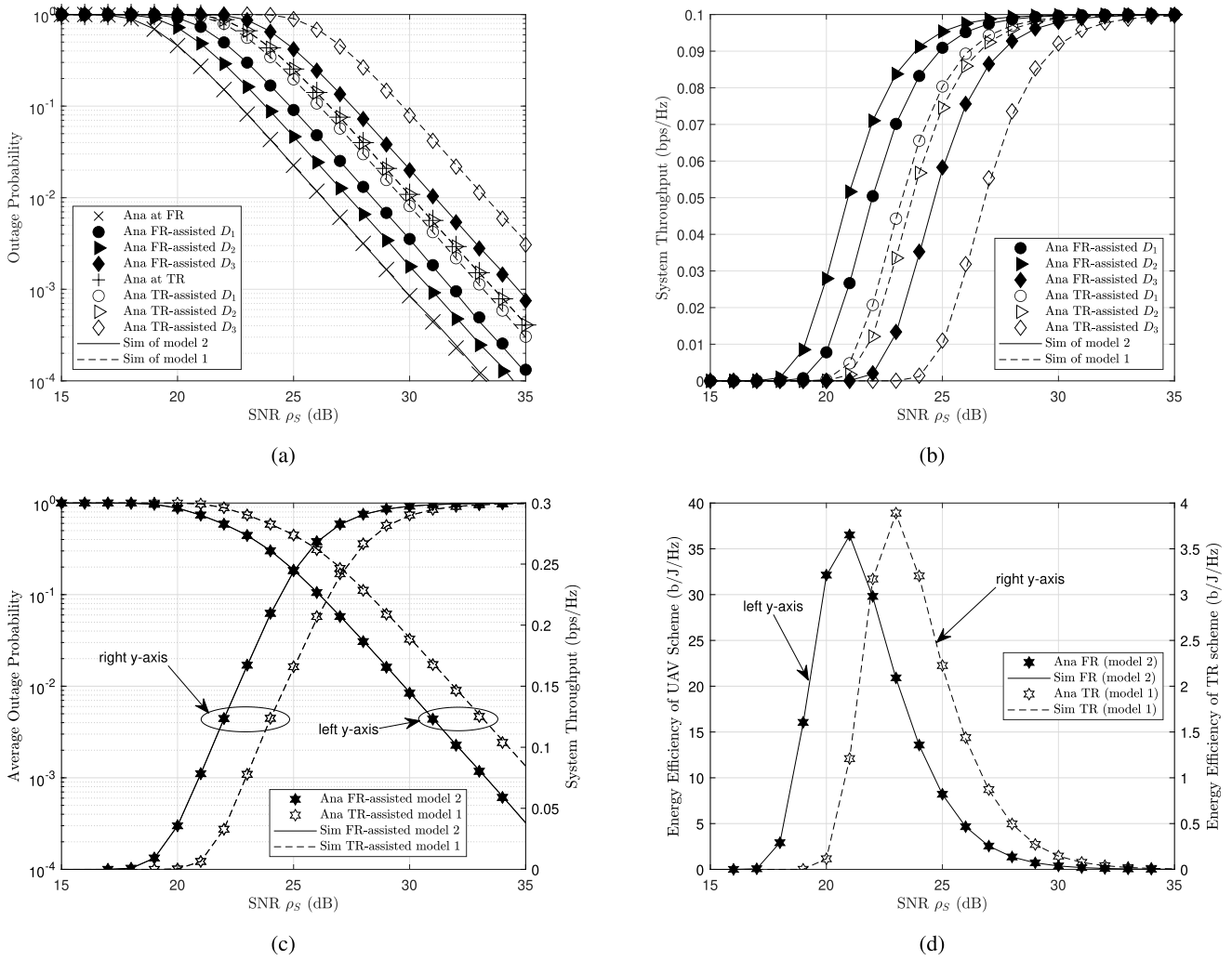

FIGURE 5. Comparisons of model 1 versus model 2 based on (a) outage probability, (b) device throughput, (c) mean of outage probability and system throughput, and (d) EE.

Figure 5a plots outage probability performance in which model 2 with FR provided outperform than model 1 TR. From Figure 5a, we obtain $OP_{U_u}^{model2} < OP_{D_2}^{model2} < OP_{D_1}^{model2} < OP_{D_3}^{model2}$ while $OP_{D_1}^{model1} < OP_{TR}^{model1} = OP_{D_2}^{model1} < OP_{D_3}^{model1}$ at most SNR. We then investigated the quality of service of devices according to their throughput $TP_{D_n}^{Q}$ bps/Hz. Based on Figure 5a, Figure 5b indicates that the throughput of the device assisted by the UAV is superior to the throughput of the device assisted by the TR. At low SNR, the throughput of D_n is given by $TP_{D_n}^{Q} = \left(1 - OP_{D_n}^{Q}\right)\mathcal{R} < \mathcal{R}$ bps/Hz since $OP_{D_n}^{Q} > 0$. The throughput of device D_n then tends toward a pre-defined bit-rate threshold $\mathcal{R}$ if the SNR tends to infinity,

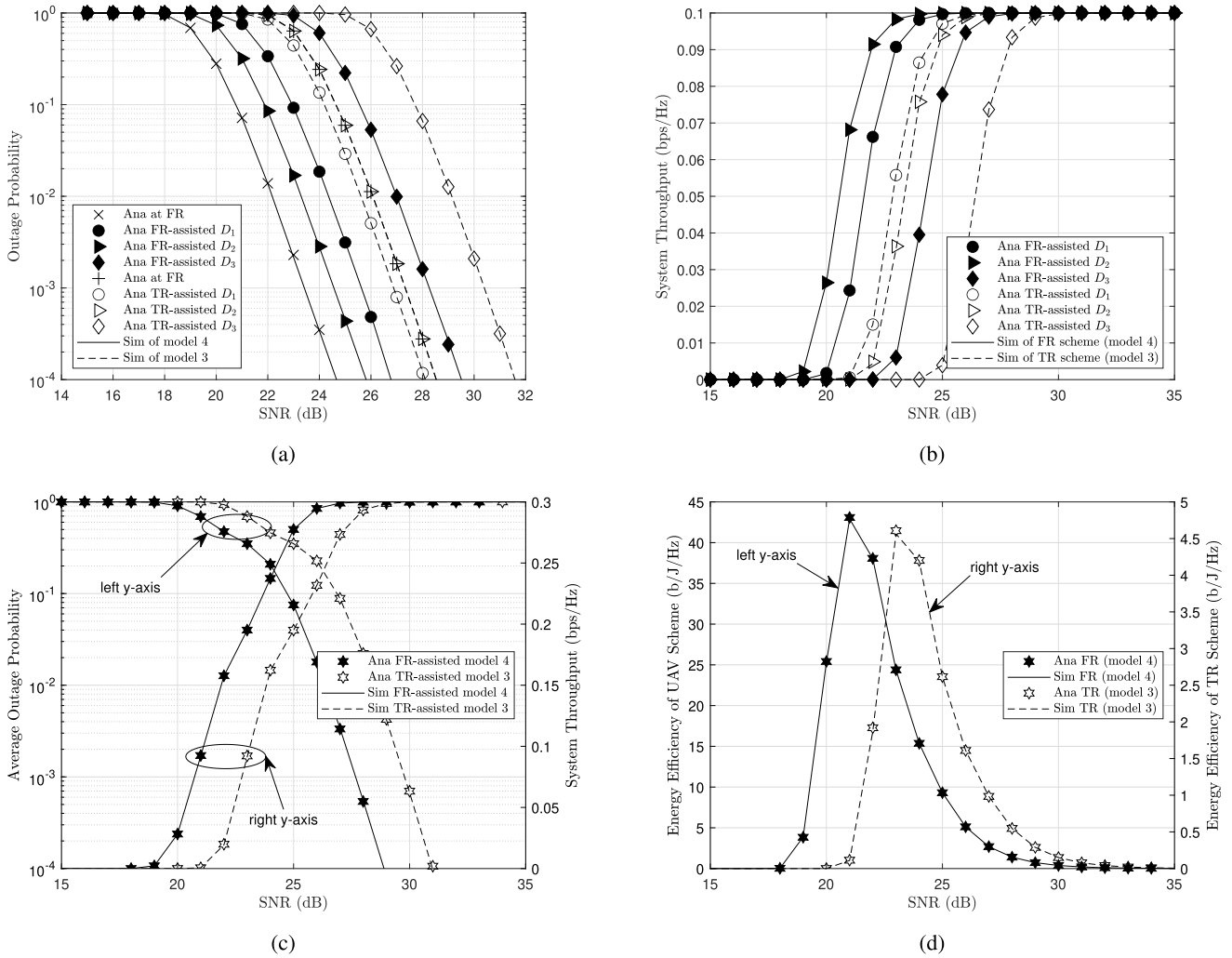

FIGURE 6. Comparisons of model 3 versus model 4 based on (a) outage probability, (b) device throughput, (c) mean of outage probability and system throughput, and (d) EE.

TABLE 4. Parameters for Monte Carlo simulations.

Expected channel gains	$\sigma_{S,U_u} = 4.6866 \times 10^{-6}$, $\sigma_{U_u,D_1} = 1.8229 \times 10^{-6}$, $\sigma_{U_u,D_2} = 6.751 \times 10^{-6}$, $\sigma_{U_u,D_3} = 2.3279 \times 10^{-7}$, $\sigma_{S,TR} = 2.1895 \times 10^{-7}$, $\sigma_{TR,D_1} = 1.5861 \times 10^{-7}$, $\sigma_{TR,D_2} = 1.2128 \times 10^{-6}$, $\sigma_{TR,D_3} = 1.1385 \times 10^{-8}$
Device bit-rate threshold	$\mathcal{R} = 0.1$ bps/Hz
PS factor	$\lambda_{U_1} = \lambda_{U_2} = 0.4$
PA factors	$\alpha_1 = 0.3333$, $\alpha_2 = 0.1667$, $\alpha_3 = 0.5$
Nakagami-m coefficient	$m = 3$
SNRs (dB)	$\rho_S = \rho_{TR}$, $\rho_{U_1} = \rho_{U_2} = \frac{1}{5}\rho_S$

i.e., $TP^{Q}_{D_n} \to \mathcal{R}$ because of $\rho_S \to +\infty$ and $OP^{Q}_{D_n} \to 0$. From Figure 5b, we obtain $TP^{model2}_{D_2} > TP^{model2}_{D_1} > TP^{model2}_{D_3}$ while $TP^{model1}_{D_1} > TP^{model1}_{D_2} > TP^{model1}_{D_3}$. To simplify the analysis of the results, we plotted the average outage probability and sum throughput for the TR and UAV schemes in the two independent scenarios as shown in Figure 5c. From equation (17) in [53], we obtained the average outage probability performance in scenario Q, where $OP^{Q}_{avg} = \frac{1}{N}\sum_{n=1}^{N} OP^{Q}_{D_n}$. In both scenarios Q, the FR-assisted NOMA-IoT scheme always delivers better quality of service to the device cluster than the TR scheme (Fig. 5c, left y-axis). The FR-assisted NOMA-IoT scheme thus provides better sum throughput performance, given by $TP^{Q}_{sum} = \sum_{n=1}^{N}\left(1 - OP^{Q}_{D_n}\right)\mathcal{R}$ bps/Hz, to the device cluster than the TR scheme (Fig. 5c, right y-axis). If SNR $\rho_S \to +\infty$, we obtain the sum throughput $TP^{Q}_{sum} = \sum_{n=1}^{N}\mathcal{R} = N\mathcal{R} = 0.3$ bps/Hz. In Figure 5d, the FR-assisted SISO-NOMA scheme consumed less energy than the TR scheme. We can clarify with a proof. The TR scheme consumes transmitting power ρ_S at the IoT hub S to transmit the superimposed signal to the TR in the first stage t_1 and then consumes transmitting power ρ_{TR} to forward the signal to devices in the second stage t_2, where $\rho_S = \rho_{TR}$. The energy consumption in the TR scheme is thus given by $EE^{Q}_{TR} = \frac{\sum_{n=1}^{N}\left(1-OP^{Q}_{D_n}(t)\right)\mathcal{R}}{\rho_S(t_1)+\rho_{TR}(t_2)}$, where $\rho_S = \rho_{TR}$. The FR scheme consumes transmitting power $\left(1-\lambda_{U_u}\right)\rho_S$ at the IoT hub S to transmit the superimposed signal from the

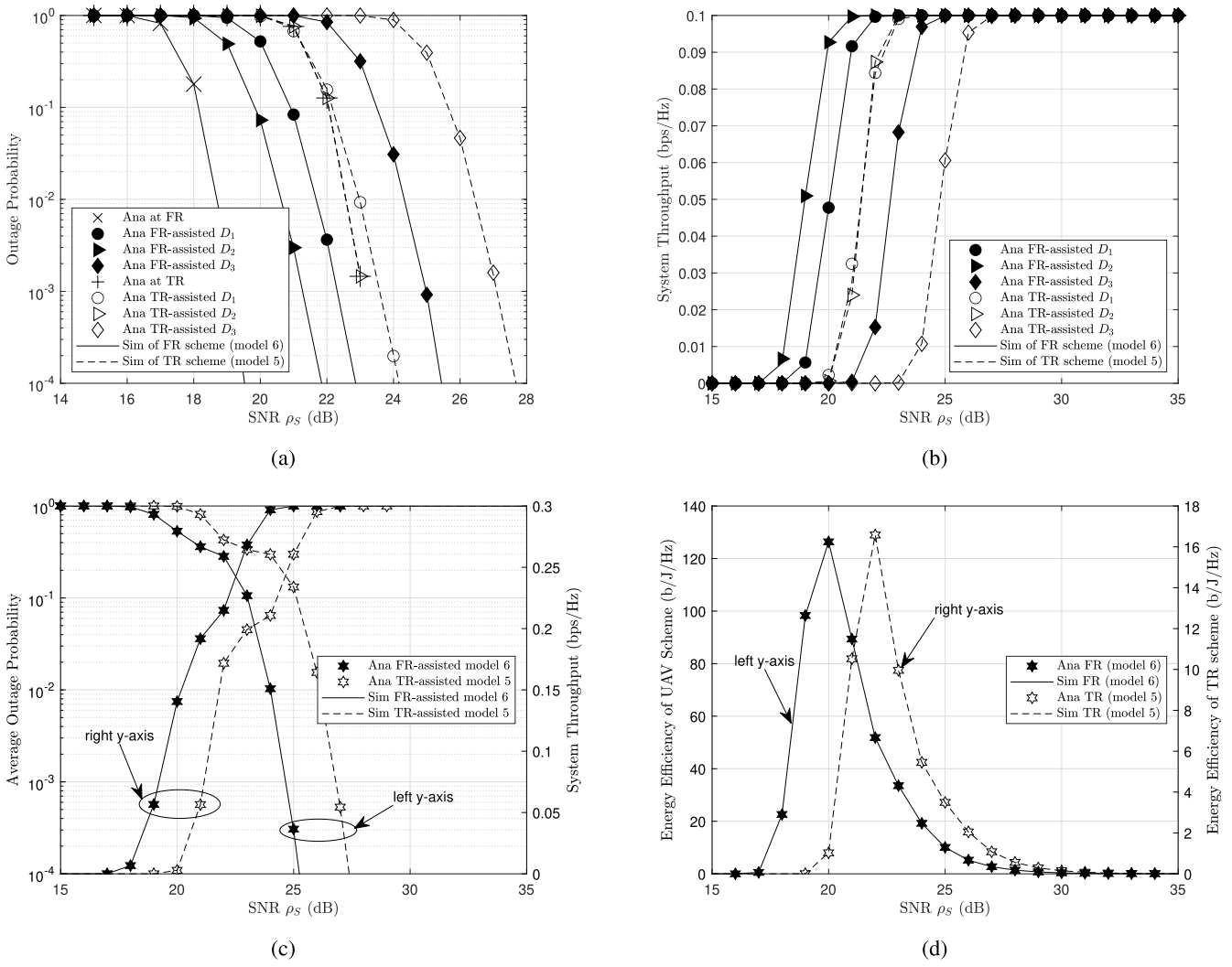

FIGURE 7. Comparisons of model 5 versus model 6 based on (a) outage probability, (b) device throughput, (c) mean of outage probability and system throughput, and (d) EE.

IoT hub S to the selected FR U_u in the first stage t_1, then consumes transmitting power ρ_{U_u} to forward the signal from the UAV U_u to devices in second stage t_2. Energy consumption in FR-UAV scheme is therefore given by $EE^Q_{FR}(t) = \frac{\sum_{n=1}^{N}\left(1-OP^Q_{D_n}(t)\right)\mathcal{R}}{(1-\lambda_{U_u})\rho_S(t_1)+\rho_{U_u}(t_2)}$, where $\rho_{U_u} = \frac{1}{5}\rho_S$. Thereby, the FR-UAV scheme (model 2) attains the best EE (Fig. 5d).

B. DISCUSSION OF MODELS 3 AND 4

In various studies, the authors conducted that Nakagami-m distribution may improve system performance (i.e., outage probability, system throughput, etc) by increasing factor $m > 1$. In this section, we also examines a SISO-IoT network, however, over Nakagami-m distributions, where factor $m = 3$. Figure 6a plots outage probability performance in which model 4 with FR-assisted SISO-IoT network provided outperform than model 3 TR. Besides, models 3 and 4 provide device throughput (Fig. 6b), system throughput (Fig. 6c), and EE (Fig. 6d) better than models 1 and 2 (Figs. 5a, 5b, 5c and 5d) since benefit of Nakagami-m ($m = 3$) distributions comparing to Rayleigh distributions.

From expressions (36), (39), (46), (47), (48), (49), (52) and (53), we observe that the outage probability of device D_n always tends toward one if the exponential function $\exp(.) = 1$. In this case, we obtain the ceiling bit-rate thresholds for devices D_3, D_1 and D_2 according to $\mathcal{R}_{D_3} = \frac{1}{2}\log_2\left(\frac{\alpha_3}{\alpha_1+\alpha_2}+1\right) = 0.5$, $\mathcal{R}_{D_1} = \frac{1}{2}\log_2\left(\frac{\alpha_1}{\alpha_2}+1\right) = 0.7923$ and $\mathcal{R}_{D_2} > 0$ bps/Hz. For clarity, we describe three cases: in the first case, if $\mathcal{R}_{D_3} \geq \frac{1}{2}\log_2\left(\frac{\alpha_3}{\alpha_1+\alpha_2}+1\right) = 0.5$ bps/Hz, devices D_3, D_1 and D_2 are forced into the probability of outage (i.e., $OP^Q_{D_3} = OP^Q_{D_1} = OP^Q_{D_2} = 1$) since the UAV relay and TR both unsuccessfully decode message x_3. Therefore, the pre-defined bit-rate threshold of device D_3 must be $\mathcal{R}_{D_3} < \frac{1}{2}\log_2\left(\frac{\alpha_3}{\alpha_1+\alpha_2}+1\right) = 0.5$ bps/Hz; in the second case, if $\mathcal{R}_{D_3} < \frac{1}{2}\log_2\left(\frac{\alpha_3}{\alpha_1+\alpha_2}+1\right) = 0.5$ but $\mathcal{R}_{D_1} \geq \frac{1}{2}\log_2\left(\frac{\alpha_1}{\alpha_2}+1\right) = 0.7923$ bps/Hz, devices D_1 and

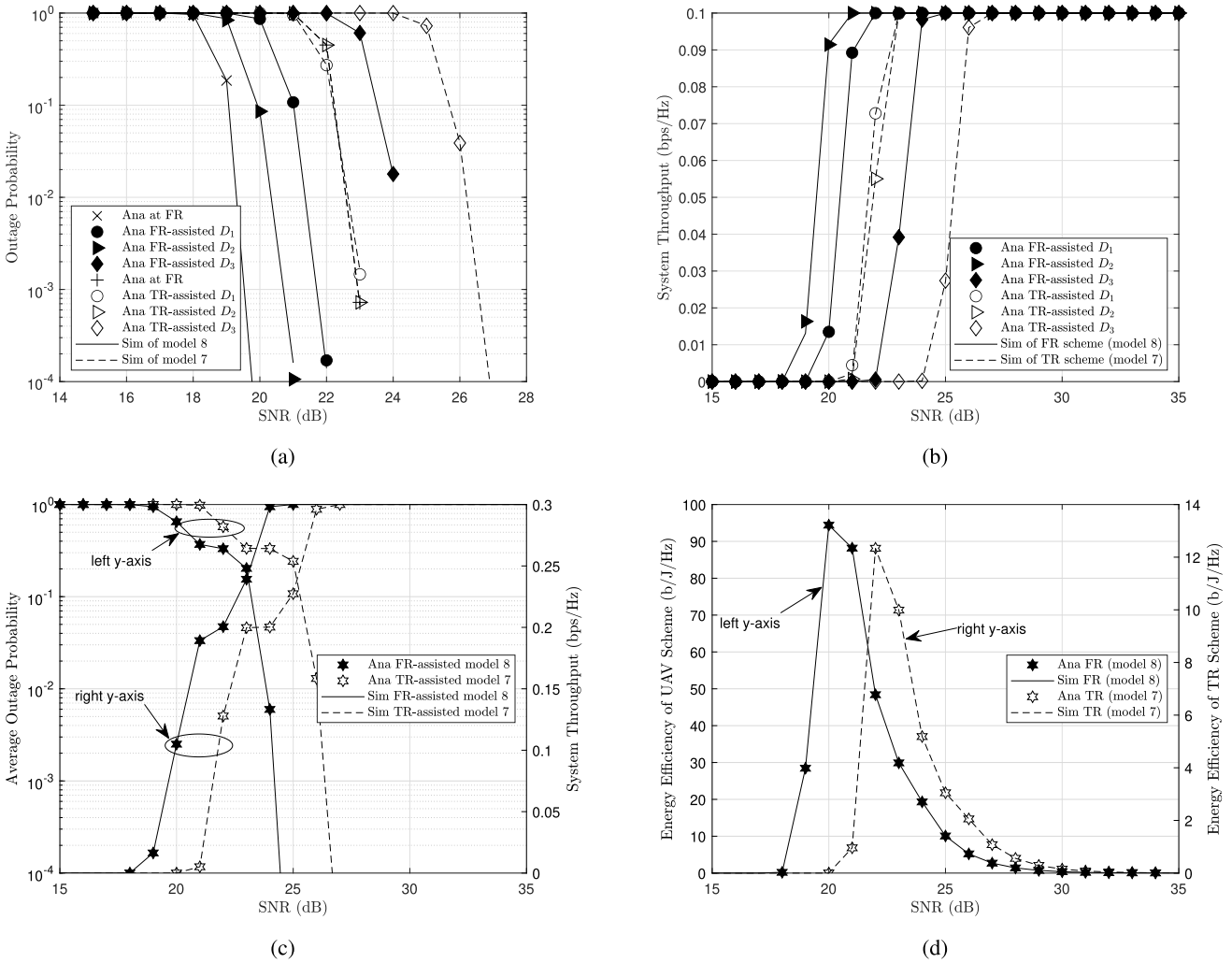

FIGURE 8. Comparisons of model 7 versus model 8 based on (a) outage probability, (b) device throughput, (c) mean of outage probability and system throughput, and (d) EE.

D_2 are forced into the probability of outage (i.e., $OP^{Q}_{D_1} = OP^{Q}_{D_2} = 1$ even SNR $\rho_S \to +\infty$) since the UAV relay, TR and devices D_1 and D_2 unsuccessfully decode message x_1; in the third case, if $\mathcal{R}_{D_3} < \frac{1}{2}\log_2\left(\frac{\alpha_3}{\alpha_1+\alpha_2}+1\right) = 0.5$ and $\mathcal{R}_{D_1} < \frac{1}{2}\log_2\left(\frac{\alpha_1}{\alpha_2}+1\right) = 0.7923$ bps/Hz, all devices D_3, D_1 and D_2 are forced into the probability of non-outage, i.e., $OP^{Q}_{D_3} \to 0$, $OP^{Q}_{D_1} \to 0$ and $OP^{Q}_{D_2} \to 0$ while SNR $\rho_S \to +\infty$. Significantly, $\mathcal{R}_{D_2} > 0$ since message x_2 is decoded without interference from other messages, and therefore $\mathcal{R}_{D_2} \to +\infty$ while SNR $\rho_S \to +\infty$. In the present study, we assigned the pre-defined bit-rate threshold $\mathcal{R} = \mathcal{R}_{D_1} = \mathcal{R}_{D_2} = R_{D_3} = 0.1$ bps/Hz, which meets the constraints $\mathcal{R}_{D_3} < \left(\frac{1}{2}\log_2\left(\frac{\alpha_3}{\alpha_1+\alpha_2}+1\right)\right) = 0.5$, $\mathcal{R}_{D_1} < \frac{1}{2}\log_2\left(\frac{\alpha_1}{\alpha_2}+1\right) = 0.7923$ and $\mathcal{R}_{D_2} > 0$ bps/Hz.

C. DISCUSSION OF MODELS 5 AND 6

In this section, we equipped multiple antennas on all IoT network nodes with $A_S = A_{U_u} = 4, A_{D_n} = 2$ for model 6 and $A_S = A_{TR} = 4, A_{D_n} = 2$ for model 5. Figures 7a, 7b, 7c, and 7d plot the outage probability, device throughput, mean outage probability and system throughput, and EE, respectively. Although the transmit power in the terrestrial scheme is greater than the transmit power in the UAV scheme, the outage probability results for the UAV scheme are superior to those of the TR scheme since the path-loss exponent factors $\varepsilon = 2$ for A2A links and $\varepsilon = 2.5$ for A2G links in the UAV scheme are lower than the path-loss exponent factor $\varepsilon = 3$ in the TR scheme, as the UAV provides a line-of-sight benefit. Comparing models 5 and 6 (MIMO over Rayleigh) to models 1 and 2 (SISO) over Rayleigh), respectively, we conclude that the MIMO technique has significantly improved the network performance compared to the SISO technique. For clarity, most devices in models 1 and 2 reached their expected bit-rate threshold $\mathcal{R} = 0.1$ bps/Hz at SNR $\rho_S = 34$ and $\rho_S = 31$ dB, respectively, as shown in Figure 6a, however, those in models 5 and 6 reached their expected bit-rate threshold $\mathcal{R} = 0.1$ bps/Hz at SNR $\rho_S = 27$ and $\rho_S = 25$ dB, respectively. Model 6 thus provided the best system throughput and EE, as shown in Figure 7d, compared to models 1, 2, 3, 4 and 5.

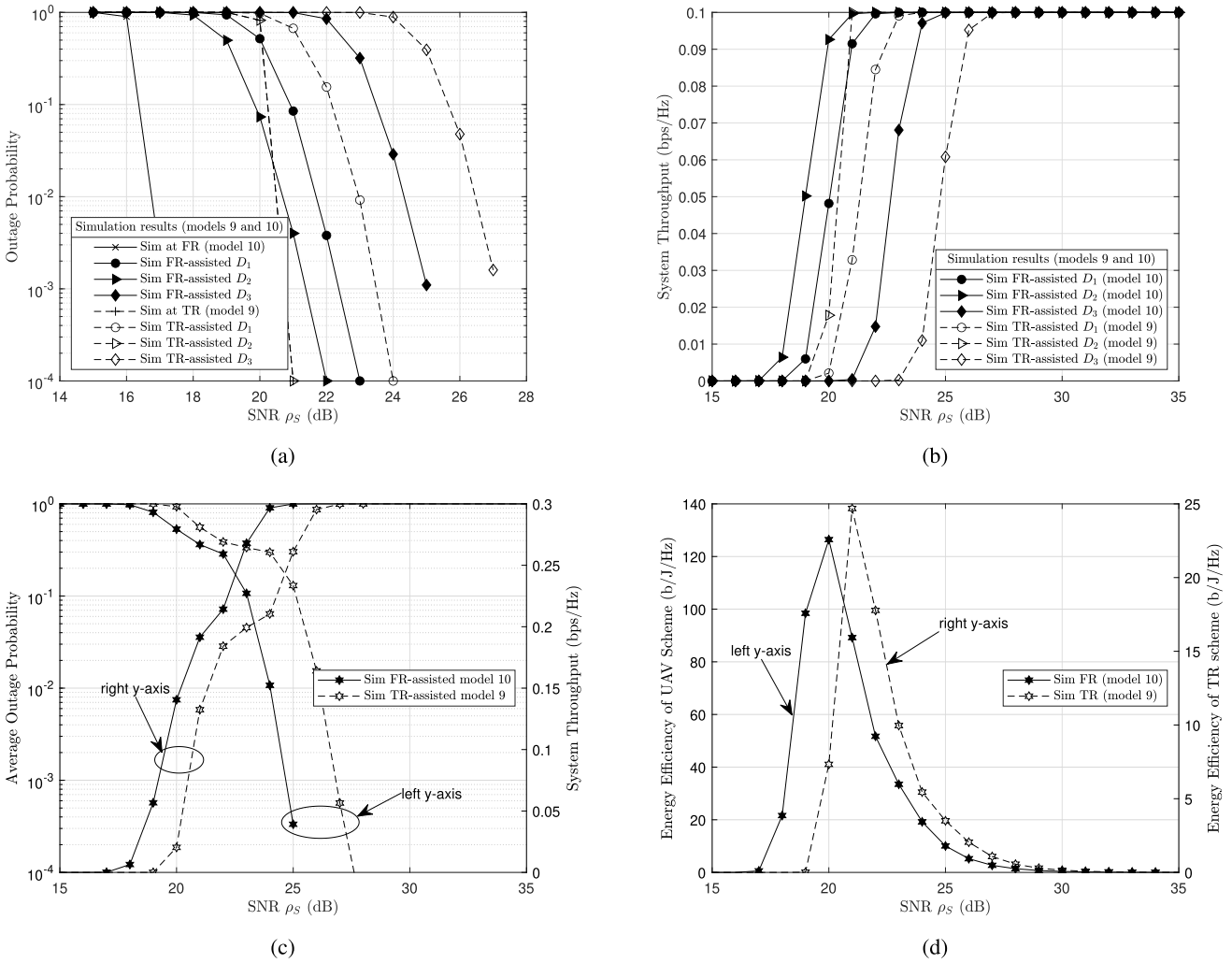

FIGURE 9. Comparisons of model 9 versus model 10 based on (a) outage probability, (b) device throughput, (c) mean of outage probability and system throughput, and (d) EE.

D. DISCUSSION OF MODELS 7 AND 8

As with models 5 and 6, we equipped multiple antennas on all IoT network nodes with $A_S = A_{U_u} = 4$, $A_{D_n} = 2$ for model 8 and $A_S = A_{TR} = 4$, $A_{D_n} = 2$ for model 7, however, distributed over Nakagami-m fading channels. Figure 8a plots outage probability of IoT devices. Notice that the outage probability results of devices in models 7 and 8 disappeared suddenly, e.g., the resulting outage probability of device D_3 in model 8 disappeared if SNR $\rho_S > 24$ dB since outage probability of device D_3 in model 8 tends to zero. As can be seen in Figure 8b, the most device throughput increases rapidly and reaches the expected rate threshold at SNR $\rho_S = 24$ dB. Besides, most devices in model 7 have reached the expected rate threshold at SNR $\rho_S = 27$ dB. As a result, models 7 and 8 provides system throughput (Fig. 8c) and EE (Fig. 8d) superior than mentioned models, i.e., models 1, 2, 3, 4, 5, and 6.

E. DISCUSSION OF MODELS 9 AND 10

Based on analysis of the results for models 1 and 2 (Fig. 5), models 3 and 4 (Fig. 6), models 5 and 6 (Fig. 7), models 7 and 8 (Fig. 8), we conclude that an increment in the number of antennas improved the system performance of the IoT network. The mMIMO technique is an upgrade evolution of the MIMO technique and employs arrays of hundreds of antennas in the network. The main advantage of the mMIMO technique is all the benefits of MIMO but on a much larger scale [54]. In this study, we present a general model and formulations for a MIMO-IoT network, and it may therefore be adapted to other schemes such as SISO and mMIMO. In this section, we equipped a large number of antennas at IoT hub S. As verification, we equipped a large number of antennas $A_S = 128$ at the IoT hub S while retaining the same number of antennas at the UAV U_u and devices, where $A_{U_u=4}$ and $A_{D_n} = 2$, respectively. The UAV and IoT devices were equipped with only a few antennas because of their small size, light weight and low cost. In this case, the pre-coding channel matrix $\mathbf{H}_{S,U_u}$ has a large size of $[A_S \times A_{U_u}] = 512$ pre-coding channels for model 10, and the pre-coding channel matrix $\mathbf{H}_{S,TR}$ has a large size of $[A_S \times A_{TR}] = 512$ pre-coding channels for model 9. The TR in model 9 has unlimited energy because it is supplied from the power grid, however,

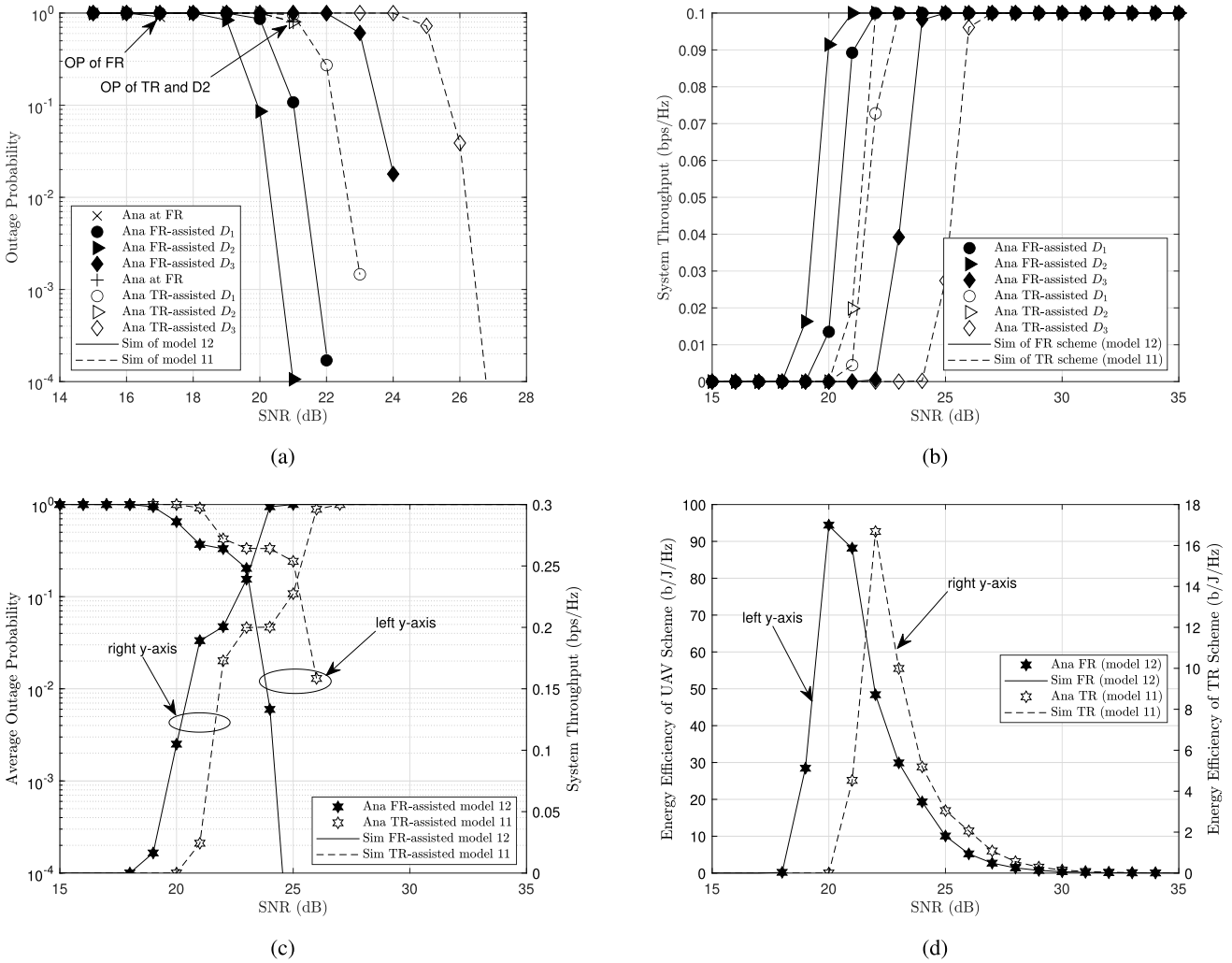

FIGURE 10. Comparisons of model 11 versus model 12 based on (a) outage probability, (b) device throughput, (c) mean of outage probability and system throughput, and (d) EE.

we equipped $A_{U_u} = A_{TR} = 4$ antennas to compare fairness. We then investigated the quality of service at devices in terms of outage probability (Fig. 9a), device throughput (Fig. 9b), mean outage probability and the sum throughput (Fig. 9c), and EE (Fig. 9d). Figure 9 plots the Monte Carlo simulations results from Algorithms 1 and , which applied (34) and (35), but an analysis of the results obtained from (36) and 39 are not presented because the factorial function of a large number of antennas returns a value which is not a number (NaN), i.e., $512! = NaN$.

Comparing the results in Figure 9 to Figures 5, 6, 7 and 8, we conclude that mMIMO improves network performance over SISO and MIMO, e.g., a comparison of the investigated results in Figure 9a (mMIMO scheme) and the results in Figures 5a and 6a (SISO) and Figures 7a and 8a (MIMO) indicates that mMIMO in combination with a large number of antennas provides better outage probability than SISO and MIMO in combination with a smaller number of antennas. We also obtained $EE^{(i)}_{TR,mMIMO} \gg EE^{(i)}_{TR,MIMO} \gg EE^{(i)}_{TR,SISO}$, but mMIMO and MIMO used in the UAV scheme provided similar EE at almost same SNR ρ_S dB, i.e. $EE^{(i)}_{FR,mMIMO} \approx EE^{(i)}_{FR,MIMO} \approx EE^{(i)}_{FR,SISO}$. It is interesting that the mMIMO technique delivers much better performance for long-distance communications in terrestrial IoT networks than the MIMO technique. However, the performance of long-distance communications in an aerial IoT network using the mMIMO technique performs slightly better than the MIMO technique. The mMIMO technique in combination with a large number of antennas also entails high hardware costs, power consumption and algorithmic complexity.

F. DISCUSSION OF MODELS 11 AND 12

Figure 10 plots the outage probability (Fig. 10a), device throughput (Fig. 10b), average outage probability and system throughput (Fig. 10c) and EE (Fig. 10d) for models 11 and 12. The outage probability of the UAV in model 12 was interrupted at SNR $\rho_S = 17$ dB, meaning that the outage probability of UAV $O^{(ii)}_{U_u,mMIMO} = 0$, where SNR $\rho_S > 17$ dB. Similarly, the outage probabilities of TR and device D_2 in model 11 were interrupted at SNR $\rho_S = 21$ dB, meaning that the outage probabilities of TR and device D_2 $O^{(ii)}_{TR,mMIMO} = O^{(ii)}_{D_2,mMIMO} = 0$, where SNR $\rho_S > 21$ dB.

Although models 11 and 12 improved the outage probability of TR and FR significantly, they only slightly improved the outage probabilities of devices compared to models 9 and 10. The average outage probability and system throughput in Figure 10c therefore approximate the average outage probability and system throughput in Figures 9c, 8c, 7c, but the average outage probability and system throughput in Figure 10c is better than the average outage probability and system throughput in Figures 6c and 5c. Figure 10d plots theEE performance of models 11 and 12. Compared to the EE performances of models 9 and 10 in Figure 9d, the EE performance in models 11 and 12 was worse than the EE performances of models 10 and 11. For example, the peak EE performance of model 11 ($EE_{TR,mMIMO}^{(Nakagami-m)} = 16.6808$ b/J/Hz at SNR $\rho_S = 22$ dB) is less than the peak EE performance of model 9 ($EE_{TR,mMIMO}^{(Rayleigh)} = 24.7792$ b/J/Hz at SNR $\rho_S = 21$ dB). Similarly, the peak EE performance of model 12 $EE_{FR,mMIMO}^{(Nakagami-m)} = 94.4008$ b/J/Hz is less than the peak EE performance of model 10 $EE_{FR,mMIMO}^{(Rayleigh)} = 127.4203$ b/J/Hz at the same SNR $\rho_S = 20$ dB. After investigating twelve individual models as shown in Table 3, we concluded that model 12 > model 11 > model 10 > model 9 > model 8 > model 7 > model 6 > model 5 > model 4 > model 3 > model 2 > model 1 based on outage probability and system throughput.

V. CONCLUSION

We comprehensively investigated a UAV-assisted NOMA-IoT wireless network and compared it to a TR-assisted NOMA-IoT wireless network. The results demonstrated an improvement in system performance by using an FR-UAV to combat fading channels and provide optimal UAV positioning through the K-means algorithm. In this manner, the expected channel gains were improved. We applied the SWIPT protocol and designed a power splitting framework to prolong UAV online time. The results also indicated that the UAV scheme which exploits line-of-sight benefits in combination with the power splitting framework delivered better performance in outage probability, system throughput and EE than a TR scheme. We derived novel closed-forms of the outage probability for Rayleigh and Nakagami-m distributions by applying the proposed max-SIC-min-rate framework and verified the theoretical results with Monte Carlo simulations. The study produced interesting conclusions: a UAV relay-assisted NOMA-IoT network is better than a TR-assisted NOMA-IoT network; the MIMO technique delivers superior system performance to the SISO technique; fading channels over Nakagami-m distributions deliver better quality of service for devices than over Rayleigh distributions; the mMIMO technique used with a large number of antennas delivers slightly better system performance than the MIMO technique in an aerial UAV relay or TR scheme, but it is more complex to implement and has higher hardware costs and consumes more energy. Although we attained valid results in the study, an open question for future research remains in how the selected UAV may use EH to forward the signal instead of using its own energy or how a resting UAV may use EH and be operated as a friendly jammer to transmit a jamming signal to block an eavesdropper. A NOMA device cluster could also be divided into multiple smaller NOMA device clusters, each served by a selected aerial relay. In this configuration, each small NOMA device cluster owns a centroid that can be determined by the K-means algorithm. From multiple centroids, the UAV trajectory follows a centroid-to-nearest-centroid path.

APPENDIX A
PROOF OF REMARK 1

In [55, Eq. (13)], the authors presented a conditional outage probability at the relay, with two messages carried in the superimposed signal. The authors also extended the cooperative model, consisting of N devices, and described the conditional outage probability at the relay in [56, Eq. (30)]. Producing Monte Carlo simulations for a large number of devices in a NOMA-IoT device cluster is challenging. We therefore employ a max-SIC-min-rate framework and obtain the conditional outage probability at the UAV U_u according to (34). We then obtain the conditional outage probability at the selected UAV U_u from the equation

$$\begin{aligned} &OP_{U_u}^{Q}(t) \\ &= 1 - \Pr\left\{ \min_{\forall x_i \in \bar{\mathbf{X}}} \max_{[A_S \times A_{U_u}]} \left\{ R_{U_u - x_i} \right\} \geq \mathcal{R} \right\} \\ &= 1 - \Pr\left\{ \max_{[A_S \times A_{U_u}]} \left\{ \left| \mathbf{H}_{S,U_u} \right|^2 \right\} \geq \frac{\gamma}{\left(1 - \lambda_{U_u}\right) \rho_S \beta} \right\}, \end{aligned} \tag{54}$$

where β in (54) is given by (38).

In Remark 1, the fading channels $h_{S,U_u}^{(a,b)} \in \mathbf{H}_{S,U_u}$ from the IoT hub S to UAV U_u occur over Rayleigh distributions, where $a \in A_S$ and $B \in A_{U_u}$. By applying the max-SIC-min-rate framework in combination with the PDF function given by (5), we obtain the outage probability at UAV U_u in scenario (i) in closed-form as follows:

$$\begin{aligned} OP_{U_u}^{(i)}(t) &= \sum_{\psi=0}^{A_S A_{U_u}} \frac{(-1)^{\psi} \left(A_S A_{U_u}\right)!}{\psi! \left(A_S A_{U_u} - \psi\right)!} \\ &\quad \times \int_{\frac{\gamma}{\left(1-\lambda_{U_u}\right)\rho_S \beta}}^{+\infty} \frac{1}{\sigma_{S,U_u}} \exp\left(-\frac{\psi x}{\sigma_{S,U_u}} \right) dx \\ &= \sum_{\psi=0}^{A_S A_{U_u}} \frac{(-1)^{\psi} \left(A_S A_{U_u}\right)!}{\psi! \left(A_S A_{U_u} - \psi\right)!} \\ &\quad \times \exp\left(-\frac{\psi \gamma}{\left(1 - \lambda_{U_u}\right) \beta \rho_S \sigma_{S,U_u}} \right), \end{aligned} \tag{55}$$

$$\text{s.t.} \quad \beta_i = \alpha_i - \gamma \sum_{j=1}^{i-1} \alpha_j, \tag{56}$$

$$\beta = \min\left\{ \beta_i \right\}. \tag{57}$$

APPENDIX B
PROOF OF REMARK 2

In Remark 2, the fading channels $h_{S,U_u}^{(a,b)} \in \mathbf{H}_{S,U_u}$ from the IoT hub S to UAV U_u occur over Rayleigh distributions, where $a \in A_S$ and $b \in A_{U_u}$. The fading channel $h_{U_u,D_n}^{(b,c)} \in \mathbf{H}_{U_u,D_n}$ from the UAV U_u to device D_n also occurs over Rayleigh distribution, where $c \in A_{D_n}$. By applying the max-SIC-min-rate framework, we obtain the outage probability at device D_n in scenario (i) in closed-form as follows:

$$\begin{aligned}
OP_{D_n}^{(i)}(t) &= 1 \\
&- \Pr\left\{ \min_{\forall x_i \geq x_n} \max_{[A_S \times A_{U_u}]} \left\{ R_{U_u - x_i}(t) \right\} \geq \mathcal{R}, \right. \\
&\qquad \left. \min_{\forall x_i \geq x_n} \max_{[A_{U_u} \times A_{D_n}]} \left\{ R_{D_n - x_i}(t) \right\} \geq \mathcal{R} \right\} \\
&= \Pr\left\{ \min_{\forall x_i \geq x_n} \left\{ \max_{[A_S \times A_{U_u}]} \left\{ R_{U_u - x_i}(t) \right\}, \right. \right. \\
&\qquad \left. \left. \max_{[A_{U_u} \times A_{D_n}]} \left\{ R_{D_n - x_i}(t) \right\} < \mathcal{R} \right\} \right\} \\
OP_{D_n}^{(i)}(t) &= 1 \\
&- \min\left\{ \Pr\left\{ \max_{[A_{U_u} \times A_{D_n}]} \left\{ \left| \mathbf{H}_{U_u,D_n} \right|^2 \right\} \geq \frac{\gamma}{\rho_{U_u} \min\limits_{\forall \alpha_i \geq \alpha_n} \{\beta_i\}} \right\}, \right. \\
&\left. \Pr\left\{ \max_{[A_S \times A_{U_u}]} \left\{ \left| \mathbf{H}_{S,U_u} \right|^2 \right\} \geq \frac{\gamma}{\left(1 - \lambda_{U_u}\right) \rho_S \min\limits_{\forall \alpha_i \geq \alpha_n} \{\beta_i\}} \right\} \right\}.
\end{aligned} \tag{58}$$

From the conditional outage probability at device D_n given by (58) in combination with the PDF given by (5), we obtain

$$\begin{aligned}
&OP_{D_n}^{(i)}(t) \\
&= \max\left\{ \sum_{\psi=0}^{A_S A_{U_u}} \frac{(-1)^\psi \left(A_S A_{U_u}\right)!}{\psi! \left(A_S A_{U_u} - \psi\right)!} \right. \\
&\qquad \times \int_{\frac{\gamma}{\left(1-\lambda_{U_u}\right) \min\limits_{\forall \alpha_i \geq \alpha_n} \{\beta_i\} \rho_S}}^{+\infty} \frac{1}{\sigma_{S,U_u}} \exp\left(-\frac{\psi x}{\sigma_{S,U_u}} \right) dx, \\
&\qquad \left. \sum_{\psi=0}^{A_{U_u} A_{D_n}} \frac{(-1)^\psi \left(A_{U_u} A_{D_n}\right)!}{\psi! \left(A_{U_u} A_{D_n} - \psi\right)!} \right. \\
&\qquad \left. \times \int_{\frac{\gamma}{\min\{\beta_i\} \rho_{U_u}}}^{+\infty} \frac{1}{\sigma_{U_u,D_n}} \exp\left(-\frac{\psi x}{\sigma_{U_u,D_n}} \right) dx \right\} \\
&= \sum_{\psi=0}^{A} \frac{(-1)^\psi A!}{\psi! (A - \psi)!} \exp\left(-\frac{\psi \gamma}{\Omega_n} \right),
\end{aligned} \tag{59}$$

$$s.t. \quad \varpi_n = \min_{\forall \alpha_i \geq \alpha_n} \left\{ \left(1 - \lambda_{U_u}\right) \beta_i \rho_S \sigma_{S,U_u} \right\}, \tag{60}$$

$$\omega_n = \min_{\forall \alpha_i \geq \alpha_n} \left\{ \beta_i \rho_{U_u} \sigma_{U_u,D_n} \right\}, \tag{61}$$

$$\Omega_n = \min\left\{ \varpi_n, \omega_n \right\}, \tag{62}$$

$$A = \begin{cases} A_S A_{U_u} \text{ for } \Omega_n = \varpi_n, \\ A_{U_u} A_{D_n} \text{ for } \Omega_n = \omega_n. \end{cases} \tag{63}$$

APPENDIX C
PROOF OF REMARK 3

In scenario (ii), the fading channel $h_{S,U_u}^{(a,b)} \in \mathbf{H}_{S,U_u}$ from the IoT hub S to UAV U_u occurs over Nakagami-m distributions, where $a \in A_S$ and $b \in A_{U_u}$. From (34) and the CDF given by (8), we obtain the outage probability at UAV U_u in closed-form as follows:

$$\begin{aligned}
OP_{U_u}^{(ii)}(t) &= \prod_{a=1}^{A_S} \prod_{b=1}^{A_{U_u}} F_{\left| h_{S,U_u}^{(a,b)} \right|^2}(x) \\
&= \prod_{a=1}^{A_S} \prod_{b=1}^{A_{U_u}} \left(1 - \exp\left(-\frac{m\gamma}{\left(1 - \lambda_{U_u}\right) \beta \rho_S \sigma_{S,U_u}} \right) \right. \\
&\qquad \left. \times \sum_{\eta=0}^{m-1} \frac{1}{\eta!} \left(\frac{m\gamma}{\left(1 - \lambda_{U_u}\right) \beta \rho_S \sigma_{S,U_u}} \right)^\eta \right),
\end{aligned} \tag{64}$$

where β is given by (57).

APPENDIX D
PROOF OF REMARK 4

In scenario (ii), the fading channels from the IoT hub S to UAVs and from UAVs to device D_n occur over two-stage Nakagami-m distributions. From (35) and the CDF given by (8), we obtain the outage probability at device D_n in closed-form as follows:

$$\begin{aligned}
&OP_{D_n}^{(ii)}(t) \\
&= \min\left\{ \prod_{a=1}^{A_S} \prod_{b=1}^{A_{U_u}} F_{\left| h_{S,U_u}^{(a,b)} \right|^2}(x), \prod_{b=1}^{A_{U_u}} \prod_{c=1}^{A_{D_n}} F_{\left| h_{U_u,D_n}^{(b,c)} \right|^2}(x) \right\} \\
&= \min\left\{ \prod_{a=1}^{A_S} \prod_{b=1}^{A_{U_u}} \left(1 - \exp\left(-\frac{m\gamma}{\varpi_n} \right) \sum_{\eta=0}^{m-1} \frac{1}{\eta!} \left(\frac{m\gamma}{\varpi_n} \right)^\eta \right), \right. \\
&\qquad \left. \prod_{b=1}^{A_{U_u}} \prod_{c=1}^{A_{D_n}} \left(1 - \exp\left(-\frac{m\gamma}{\omega_n} \right) \sum_{\eta=0}^{m-1} \frac{1}{\eta!} \left(\frac{m\gamma}{\omega_n} \right)^\eta \right) \right\} \\
&= \prod_{\psi=1}^{A} \left(1 - \exp\left(-\frac{m\gamma}{\Omega_n} \right) \sum_{\eta=0}^{m-1} \frac{1}{\eta!} \left(\frac{m\gamma}{\Omega_n} \right)^\eta \right),
\end{aligned} \tag{65}$$

where ϖ_n, ω_n, Ω_n and A are given by (40), (41), (42) and (43), respectively.

ACKNOWLEDGMENT

The authors deeply thank Soundararajan Ezekiel (sezekiel@iup.edu) from the Department of Computer Science, Indiana University of Pennsylvania, when he visited Ton Duc Thang University for its 25th anniversary for his helpful advice in improving this paper.

REFERENCES

[1] K. Shafique, B. A. Khawaja, F. Sabir, S. Qazi, and M. Mustaqim, "Internet of Things (IoT) for next-generation smart systems: A review of current challenges, future trends and prospects for emerging 5G-IoT scenarios," *IEEE Access*, vol. 8, pp. 23022–23040, 2020.

[2] J. Wang, K. Zhu, and E. Hossain, "Green Internet of Vehicles (IoV) in the 6G era: Toward sustainable vehicular communications and networking," *IEEE Trans. Green Commun. Netw.*, vol. 6, no. 1, pp. 391–423, Mar. 2022.

[3] A. Mahmoud, S. Muhaidat, P. C. Sofotasios, I. Abualhaol, O. A. Dobre, and H. Yanikomeroglu, "Intelligent reflecting surfaces assisted UAV communications for IoT networks: Performance analysis," *IEEE Trans. Green Commun. Netw.*, vol. 5, no. 3, pp. 1029–1040, Sep. 2021.

[4] S. Zeadally, M. A. Javed, and E. B. Hamida, "Vehicular communications for ITS: Standardization and challenges," *IEEE Commun. Stand. Mag.*, vol. 4, no. 1, pp. 11–17, Dec. 2020.

[5] B. Zong, C. Fan, X. Wang, X. Duan, B. Wang, and J. Wang, "6G technologies: Key drivers, core requirements, system architectures, and enabling technologies," *IEEE Veh. Technol. Mag.*, vol. 14, no. 3, pp. 18–27, Sep. 2019.

[6] M. Shi, K. Yang, Z. Han, and D. Niyato, "Coverage analysis of integrated sub-6 GHz-mmWave cellular networks with hotspots," *IEEE Trans. Commun.*, vol. 67, no. 11, pp. 8151–8164, Nov. 2019.

[7] Y. Jing and H. Jafarkhani, "Single and multiple relay selection schemes and their achievable diversity orders," *IEEE Trans. Wireless Commun.*, vol. 8, no. 3, pp. 1414–1423, Mar. 2009.

[8] S. Lee, D. B. da Costa, Q.-T. Vien, T. Q. Duong, and R. T. de Sousa, "Non-orthogonal multiple access schemes with partial relay selection," *IET Commun.*, vol. 11, no. 6, pp. 846–854, 2017.

[9] K. Guo, D. Guo, and B. Zhang, "Performance analysis of two-way multi-antenna multi-relay networks with hardware impairments," *IEEE Access*, vol. 5, pp. 15971–15980, 2017.

[10] K. Guo, K. An, B. Zhang, and D. Guo, "Performance analysis of two-way satellite multi-terrestrial relay networks with hardware impairments," *Sensors*, vol. 18, vol 5, p. 1574, May 2018.

[11] K. Guo, M. Lin, B. Zhang, J. Ouyang, and W.-P. Zhu, "Secrecy performance of satellite wiretap channels with multi-user opportunistic scheduling," *IEEE Wireless Commun. Lett.*, vol. 7, no. 6, pp. 1054–1057, Dec. 2018.

[12] K. Guo, K. An, B. Zhang, Y. Huang, D. Guo, G. Zheng, and S. Chatzinotas, "On the performance of the uplink satellite multiterrestrial relay networks with hardware impairments and interference," *IEEE Syst. J.*, vol. 13, no. 3, pp. 2297–2308, Sep. 2019.

[13] X. Tang, K. An, K. Guo, S. Wang, X. Wang, J. Li, and F. Zhou, "On the performance of two-way multiple relay non-orthogonal multiple access-based networks with hardware impairments," *IEEE Access*, vol. 7, pp. 128896–128909, 2019.

[14] Y.-C. Ko, M. S. Alouini, and M. K. Simon, "Analysis and optimization of switched diversity systems," *IEEE Trans. Veh. Technol.*, vol. 49, no. 5, pp. 1813–1831, Sep. 2000.

[15] B. S. Tan, K. H. Li, and K. C. Teh, "Analysis of switch diversity combining over two wave with diffuse power fading," *IET Commun.*, vol. 6, no. 9, pp. 1061–1067, Jun. 2012.

[16] M. Yang, D. Guo, Y. Huang, T. Q. Duong, and B. Zhang, "Secure multiuser scheduling in downlink dual-hop regenerative relay networks over Nakagami-*m* fading channels," *IEEE Trans. Wireless Commun.*, vol. 15, no. 12, pp. 8009–8024, Dec. 2016.

[17] X. Yu, J. Cai, M. Xie, and T. Teng, "Ergodic rate analysis of massive spatial modulation MIMO system with NOMA in cooperative relay networks," *IEEE Syst. J.*, vol. 16, no. 3, pp. 4513–4524, Sep. 2022.

[18] V. Dixit and A. Kumar, "An exact error analysis of multi-user RC/MRC based MIMO-NOMA-VLC system with imperfect SIC," *IEEE Access*, vol. 9, pp. 136710–136720, 2021.

[19] M. Mozaffari, W. Saad, M. Bennis, Y.-H. Nam, and M. Debbah, "A tutorial on UAVs for wireless networks: Applications, challenges, and open problems," *IEEE Commun. Surveys Tuts.*, vol. 21, no. 3, pp. 2334–2360, 3rd Quart., 2019.

[20] D. Liu, Y. Xu, J. Wang, J. Chen, K. Yao, Q. Wu, and A. Anpalagan, "Opportunistic UAV utilization in wireless networks: Motivations, applications, and challenges," *IEEE Commun. Mag.*, vol. 58, no. 5, pp. 62–68, May 2020.

[21] X. Chen, X. Hu, Q. Zhu, W. Zhong, and B. Chen, "Channel modeling and performance analysis for UAV relay systems," *China Commun.*, vol. 15, no. 12, pp. 89–97, Dec. 2018.

[22] S. Zhang, H. Zhang, Q. He, K. Bian, and L. Song, "Joint trajectory and power optimization for UAV relay networks," *IEEE Commun. Lett.*, vol. 22, no. 1, pp. 161–164, Jan. 2018.

[23] W. Wang, X. Li, M. Zhang, K. Cumanan, D. W. K. Ng, G. Zhang, J. Tang, and O. A. Dobre, "Energy-constrained UAV-assisted secure communications with position optimization and cooperative jamming," *IEEE Trans. Commun.*, vol. 68, no. 7, pp. 4476–4489, Jul. 2020.

[24] B. Li, Z. Fei, and Y. Zhang, "UAV communications for 5G and beyond: Recent advances and future trends," *IEEE Internet Things J.*, vol. 6, no. 2, pp. 2241–2263, Apr. 2019.

[25] R. Shahzadi, M. Ali, H. Z. Khan, and M. Naeem, "UAV assisted 5G and beyond wireless networks: A survey," *J. Netw. Comput. Appl.*, vol. 189, Sep. 2021, Art. no. 103114.

[26] Y. Zeng and R. Zhang, "Energy-efficient UAV communication with trajectory optimization," *IEEE Trans. Wireless Commun.*, vol. 16, no. 6, pp. 3747–3760, Jun. 2016.

[27] Y. Zeng, R. Zhang, and T. J. Lim, "Throughput maximization for UAV-enabled mobile relaying systems," *IEEE Trans. Commun.*, vol. 64, no. 12, pp. 4983–4996, Dec. 2016.

[28] Y. Guo, C. You, C. Yin, and R. Zhang, "UAV trajectory and communication co-design: Flexible path discretization and path compression," *IEEE J. Sel. Areas Commun.*, vol. 39, no. 11, pp. 3506–3523, Nov. 2021.

[29] A. Liu and V. K. N. Lau, "Optimization of multi-UAV-aided wireless networking over a ray-tracing channel model," *IEEE Trans. Wireless Commun.*, vol. 18, no. 9, pp. 4518–4530, Sep. 2019.

[30] L. Li, T. Chang, and S. Cai, "UAV positioning and power control for two-way wireless relaying," *IEEE Trans. Wireless Commun.*, vol. 19, no. 2, pp. 1008–1024, Feb. 2020.

[31] C. Guo, J. Xin, L. Zhao, and X. Chu, "Performance analysis of cooperative NOMA with energy harvesting in multi-cell networks," *China Commun.*, vol. 16, no. 11, pp. 120–129, Nov. 2019.

[32] C. In, H.-M. Kim, and W. Choi, "Achievable rate-energy region in two-way decode-and-forward energy harvesting relay systems," *IEEE Trans. Commun.*, vol. 67, no. 6, pp. 3923–3935, Jun. 2019.

[33] T. D. P. Perera and D. N. K. Jayakody, "Analysis of time-switching and power-splitting protocols in wireless-powered cooperative communication system," *Phys. Commun.*, vol. 31, pp. 141–151, Dec. 2018.

[34] J. Tang, J. Luo, M. Liu, D. K. C. So, E. Alsusa, G. Chen, K.-K. Wong, and J. A. Chambers, "Energy efficiency optimization for NOMA with SWIPT," *IEEE J. Sel. Topics Signal Process.*, vol. 13, no. 3, pp. 452–466, Jun. 2019.

[35] T.-N. Tran, V.-C. Ho, T. P. Vo, K. N. N. Tran, and M. Voznak, "Design of relay switching to combat an eavesdropper in IoT-NOMA wireless networks," *Future Internet*, vol. 14, no. 3, p. 71, Feb. 2022.

[36] N. Zhao, W. Lu, M. Sheng, Y. Chen, J. Tang, F. R. Yu, and A.-K. Wong, "UAV-assisted emergency networks in disasters," *IEEE Wireless Commun.*, vol. 26, no. 1, pp. 45–51, Feb. 2019.

[37] N.-P. Nguyen, T. Q. Duong, H. Q. Ngo, Z. Hadzi-Velkov, and L. Shu, "Secure 5G wireless communications: A joint relay selection and wireless power transfer approach," *IEEE Access*, vol. 4, pp. 3349–3359, 2016.

[38] Q. Wu, Y. Zeng, and R. Zhang, "Joint trajectory and communication design for multi-UAV enabled wireless networks," *IEEE Trans. Wireless Commun.*, vol. 17, no. 3, pp. 2109–2121, Mar. 2018.

[39] M. Alazab, K. Lakshmanna, Q.-V. Pham, and P. K. R. Maddikunta, "Multi-objective cluster head selection using fitness averaged rider optimization algorithm for IoT networks in smart cities," *Sustain. Energy Technol. Assessments*, vol. 43, Feb. 2021, Art. no. 100973.

[40] P. S. Rathore, J. M. Chatterjee, A. Kumar, and R. Sujatha, "Energy-efficient cluster head selection through relay approach for WSN," *J. Supercomput.*, vol. 77, no. 7, pp. 7649–7675, Jul. 2021.

[41] H. Wu, Y. Wen, J. Zhang, Z. Wei, N. Zhang, and X. Tao, "Energy-efficient and secure air-to-ground communication with jittering UAV," *IEEE Trans. Veh. Technol.*, vol. 69, no. 4, pp. 3954–3967, Apr. 2020.

[42] İ. Baştürk, "Energy-efficient communication for UAV-enabled mobile relay networks," *Comput. Netw.*, vol. 213, Aug. 2022, Art. no. 109071.

[43] N.-L. Nguyen, S.-P. Le, A.-T. Le, N. D. Nguyen, D.-T. Do, and M. Voznak, "UAV based satellite-terrestrial systems with hardware impairment and imperfect SIC: Performance analysis of user pairs," *IEEE Access*, vol. 9, pp. 117925–117937, 2021.

[44] J. Zheng, "Fast receive antenna subset selection for pre-coding aided spatial modulation," *IEEE Commun. Lett.*, vol. 4, no. 3, pp. 317–320, Jun. 2015.

[45] F. Chen, K. Yang, P. Xing, H. Zhang, and Y. Jiang, "Multiuser pre-coding aided quadrature spatial modulation for large-scale MIMO channels," *China Commun.*, vol. 15, no. 11, pp. 62–69, Nov. 2018.
[46] D. Liao, H. Li, G. Sun, M. Zhang, and V. Chang, "Location and trajectory privacy preservation in 5g-enabled vehicle social network services," *J. Netw. Comput. Appl.*, vol. 110, pp. 108–118, Oct. 2018.
[47] X. Lu, P. Wang, D. Niyato, D. I. Kim, and Z. Han, "Wireless networks with RF energy harvesting: A contemporary survey," *IEEE Commun. Surveys Tuts.*, vol. 17, no. 2, pp. 757–789, 2nd Quart., 2015.
[48] T.-N. Tran, M. Voznak, P. Fazio, and V.-C. Ho, "Emerging cooperative MIMO-NOMA networks combining TAS and SWIPT protocols assisted by an AF-VG relaying protocol with instantaneous amplifying factor maximization," *AEU-Int. J. Electron. Commun.*, vol. 135, Jun. 2021, Art. no. 153695.
[49] T.-N. Tran, T. P. Vo, P. Fazio, and M. Voznak, "SWIPT model adopting a PS framework to aid IoT networks inspired by the emerging cooperative NOMA technique," *IEEE Access*, vol. 9, pp. 61489–61512, 2021.
[50] T. Tran and M. Voznak, "Adaptive multiple access assists multiple users over multiple-input-multiple-output non-orthogonal multiple access wireless networks," *Int. J. Commun. Syst.*, vol. 34, no. 10, p. e4803, Jul. 2021.
[51] T.-N. Tran and M. Voznak, "On secure system performance over SISO, MISO and MIMO-NOMA wireless networks equipped a multiple antenna based on TAS protocol," *EURASIP J. Wireless Commun. Netw.*, vol. 2020, no. 1, pp. 1–22, Dec. 2020.
[52] Z. Ding, Z. Yang, P. Fan, and H. V. Poor, "On the performance of non-orthogonal multiple access in 5G systems with randomly deployed users," *IEEE Signal Process. Lett.*, vol. 21, no. 12, pp. 1501–1505, Dec. 2014.
[53] H. Lei, J. Zhang, K.-H. Park, P. Xu, I. S. Ansari, G. Pan, B. Alomair, and M.-S. Alouini, "On secure NOMA systems with transmit antenna selection schemes," *IEEE Access*, vol. 5, pp. 17450–17464, 2017.
[54] A. Gupta and R. K. Jha, "A survey of 5G network: Architecture and emerging technologies," *IEEE Access*, vol. 3, pp. 1206–1232, 2015.
[55] Y. Liu, Z. Ding, M. Elkashlan, and H. V. Poor, "Cooperative non-orthogonal multiple access with simultaneous wireless information and power transfer," *IEEE J. Sel. Areas Commun.*, vol. 34, no. 4, pp. 938–953, Apr. 2016.
[56] T.-N. Tran and M. Voznak, "Switchable coupled relays aid massive non-orthogonal multiple access networks with transmit antenna selection and energy harvesting," *Sensors*, vol. 21, no. 4, p. 1101, Feb. 2021.

THANH-NAM TRAN was born in Vinh Long, Vietnam, in 1988. He received the M.Sc. degree in information systems from Military Technical Academy (MTA), in 2014, and the Ph.D. degree in communications technology from the Faculty of Electrical Engineering and Computer Science, Technical University of Ostrava (VSB-TOU), Czech Republic, in 2021. He is currently a Junior Researcher at the Research and Development Team of Prof. Miroslav Voznak, VSB-TOU. He works for the Faculty of Information Technology, Ton Duc Thang University, where he also serves as a Senior Member of the Data Science Research Group. His research interests include wireless communication networks, data science, and AI.

THANH-LONG NGUYEN received the bachelor's degree in information technology from the University of Science, Ho Chi Minh City, in 2003, the master's degree in computer science from Hue University, Thua Thien Hue, Vietnam, in 2011, and the Ph.D. degree from the VSB-Technical University of Ostrava, Czech Republic, in 2021. He is currently a Lecturer and a Researcher and serves as the Vice Dean at the Faculty of Information Technology, Ho Chi Minh City University of Food Industry. His research interests include applied informatics, knowledge discovery, data mining, and information and communications technologies.

MIROSLAV VOZNAK (Senior Member, IEEE) was born in Czechia, in 1971. He received the Ph.D. degree in telecommunications from the Faculty of Electrical Engineering and Computer Science, Technical University of Ostrava, in 2002, and the Habilitation degree, in 2009. He was appointed as a Full Professor in electronics and communications technologies, in 2017. He is the author or coauthor of more than 100 articles in SCI/SCIE journals. His research interests include information and communications technology, especially quality of service and experience, network security, wireless networks, and in recent years, big data analytics. He served as the General Chair at scientific conferences, such as IEEE/ACM DS-RT, in 2020, and IFIP WMNC, in 2018. He is one of the World's Top 2% Scientists listed by Stanford University.